

Rheology and thermomechanical evaluation of additively manufactured acrylonitrile butadiene styrene (ABS) with optimized tungsten carbide (WC) nano-ceramic content



Nectarios Vidakis ^{a,*}, Amalia Moutsopoulou ^a, Markos Petousis ^a, Nikolaos Michailidis ^{b,c}, Chrysa Charou ^a, Vassilis Papadakis ^{d,e}, Nikolaos Mountakis ^a, Evgenia Dimitriou ^{b,c}, Apostolos Argyros ^{b,c}

^a Department of Mechanical Engineering, Hellenic Mediterranean University, Heraklion, 71410, Greece

^b Physical Metallurgy Laboratory, Mechanical Engineering Department, School of Engineering, Aristotle University of Thessaloniki, 54124, Thessaloniki, Greece

^c Centre for Research & Development of Advanced Materials (CERDAM), Center for Interdisciplinary Research and Innovation, Balkan Centre, Building B', 10th km Thessaloniki-Thermi road, 57001, Thessaloniki, Greece

^d Department of Industrial Design and Production Engineering, University of West Attica, 122 43, Athens, Greece

^e Institute of Electronic Structure and Laser of the Foundation for Research and Technology-Hellas (IESL-FORTH) – Hellas, N. Plastira 100m, 70013, Heraklion, Greece

ARTICLE INFO

Handling Editor: Dr P. Vincenzini

Keywords:

Material extrusion (MEX) 3D printing
Acrylonitrile butadiene styrene (ABS)
Tungsten carbide (WC)
Nanocomposites

ABSTRACT

Tungsten carbide (WC), a superhard and thermally stable ceramic, is widely used in several industries. Its exceptional features portray WC as a promising reinforcement and stabilizing agent for popular polymeric matrices deployed in material extrusion (MEX) 3D-Printing, such as Acrylonitrile Butadiene Styrene (ABS). This potential was investigated in depth and is presented herein. ABS/WC nanocomposite filaments were prepared by melt extrusion and tested. A filler loading of 0 wt % up to 10 wt % WC, in 2 wt % steps were fabricated. The impact of the WC nanopowder content on the structural, rheological, thermal, mechanical, and morphological characteristics of nanocomposite filaments and 3D printed samples was investigated with the aid of fifteen (15) different tests. The experiments revealed excellent thermal stability of the developed nanocomposites, as well as non-Newtonian shear thinning behavior of their melts, which is encouraging for their processability. WC nanoparticles impressively upgraded the mechanical capacity of the optimized nanocomposites in comparison to that of pure ABS. ABS with 4.0 wt % WC grade exhibited a noticeable increase in most of the mechanical characteristics; Compressive, flexural, and tensile strength all rose by 25.9%, 29.4%, and 20.9% respectively, while the microhardness increased by 100.3%, showing potential for use in applications requiring high wear resistance. The findings of the current research indicate that novel cost-effective ABS/WC composites have high potential and industrial merit for a variety of demanding applications with ABS-based composites.

1. Introduction

Additive manufacturing has advanced notably over the past decade and is now widely utilized in several sectors that are important to human life, such as food and living tissues, as well as in the manufacturing of engine parts and spares [1]. Among the various additive manufacturing methods, fused filament fabrication (FFF) is widely acknowledged as the most commonly employed technique for 3D printing with polymers [2]. As 3D printing becomes more widely available, there is an increasing

need for materials that can ensure the long-term durability and exceptional mechanical properties of 3D printed products [1]. Ceramics have a wide range of uses in a plethora of industries because of their cutting-edge and adaptable qualities [3]. Recently, the utilization of ceramic-polymer composites has increased, as these materials offer special features that cannot be obtained by 3D printing of pure thermoplastic filaments. These composite materials exhibit high hardness, wear resistance, electrical conductivity, and other beneficial characteristics [4]. Recent studies have shown that modest amounts of fine

* Corresponding author.

E-mail addresses: vidakis@hmu.gr (N. Vidakis), amalia@hmu.gr (A. Moutsopoulou), markospetousis@hmu.gr (M. Petousis), nmichail@auth.gr (N. Michailidis), charou@hmu.gr (C. Charou), v.papadakis@uniwa.gr (V. Papadakis), mountakis@hmu.gr (N. Mountakis), evgeniaod@auth.gr (E. Dimitriou), aargyros@auth.gr (A. Argyros).

ceramic powder can significantly alter the characteristics of 3D-printed objects. These modifications resulted in a notable improvement in the strength of 3D-printed objects and a discernible decrease in the rate of wear [5].

Carbides are ceramics with impressive mechanical properties, particularly against wear; therefore, they are used in coatings and cutting tools [6,7]. Owing to its outstanding characteristics such as chemical stability, resistance to high temperatures, high strength, and low density, tungsten carbide (WC) is highly valued and preferred for a variety of applications [8]. The addition of tungsten carbide (WC) powder enhanced the anti-abrasion and mechanical behavior of the composite materials. One study incorporated silicon powder and WC powder into a glass/epoxy composite, demonstrating a notable improvement in wear resistance [9]. The effects of adding WC powder to glass/epoxy composites were also examined, showing that the tribological behavior of the composites improved as a result of the inclusion of WC powder [10]. In the case of material extrusion (MEX) Additive Manufacturing (AM) technology, research remains relatively limited, and to the best of the authors' knowledge, the incorporation of WC as reinforcement in nanocomposites has not yet been accomplished.

In the research topic of investigating properties of polymers 3D printed utilizing the FFF technique, which is a MEX 3D printing technique, a notable amount of research has concentrated on materials made of acrylonitrile butadiene styrene (ABS) [11]. This is mainly because ABS is user-friendly for 3D printing and has a comparatively low melting point of approximately 200 °C [12]. ABS possesses numerous beneficial characteristics that make it ideal for printing applications, including lightweight, chemical inertness, eco-friendliness, and recycling capacity [12]. In addition to its extraordinary resistance to impacts and scratches, ABS also exhibits outstanding mechanical properties, such as strength and toughness [13]. It is the second-most frequently employed polymer in 3D printing using fused filament fabrication (FFF) [14]. Its sustainability has also been reported and promising results have been obtained [15]. As a result, extensive research has been conducted to examine how well it performs during and after printing, with the effect of the 3D printing setting on its performance being a common task in the literature [16]. Numerous tests have been conducted to thoroughly determine the mechanical characteristics of ABS, including tensile tests with varying strain rates [17], creep and fatigue loads [18], flexural investigations employing statistical modeling techniques [19], Dynamic Mechanical Analysis (DMA) [20], and impact loading analyses [21].

Furthermore, compounds have been created using ABS as a polymer matrix and nanoscale (or rarely microscale) fillers to enhance the mechanical characteristics of ABS and provide multifunctional qualities. These composites aim to improve specific qualities such as the mechanical or electrical properties of the material [22,23]. These additions consist of glass fibers [24,25] carbon-based additives such as graphene single- and multi-wall carbon nanotubes [26,27] ceramics such as titanium nitride [13] metals such as copper [28,29] metal oxides such as antimony and titanium oxide [30,31] ferric oxide [32] and zinc oxide [30,33]. Ceramic additives in nanopowder forms, such as Titanium Nitrate (TiN) [13] and Silicon Nitrate (Si_3N_4) [34], provide significant mechanical strengthening over pure ABS. However, the use of ceramic nanoparticles (NPs) for enhancement of MEX 3D-printing by the development of nanocompounds with polymeric matrices is still limited [35], although, as mentioned, the need for materials with improved performance in AM is high. Regarding the electrical properties mentioned above, the literature reports that the addition of WC drastically reduces the electrical conductivity of composites [36]. This was also verified in the current study, with WC nanopowder electrical conductivity measurements showing that it was not conductive and, as expected, similar to the 3D printed samples. Therefore, this study focused on the mechanical properties of 3D-printed samples.

This study consisted of multiple parts. First, the extrusion settings for the synthesis of polymer-ceramic filaments were investigated, and the incorporation of tungsten carbide particles into ABS was assessed. The

thermal characteristics of the filaments produced were investigated via thermogravimetric analysis (TGA) and Differential Scanning Calorimetry (DSC), and the rheological behavior of the filaments above their melting point was examined. Furthermore, Scanning Electron Microscopy (SEM), energy-dispersive spectroscopy (EDS), and Raman analyses were performed to inspect the chemical structures of the compounds. Next, the mechanical properties of 3D printed specimens were evaluated, and SEM and Atomic Force Microscopy (AFM) were used to investigate the surface microstructures of the samples. Finally, the potential of the composites for MEX 3D printing applications was discussed. The composites discussed in this study have not only enhanced the tensile strength but have also exhibited a remarkable increase in microhardness measurements (an impressive 100.3% improvement). These advancements make these materials well-suited for applications that demand performance criteria related to wear resistance because hardness affects the quality of the material (wear resistance) [37,38].

2. Materials & methods

The fabrication and testing processes for the synthesis of filaments, 3D printing of specimens, and measurements are displayed in Fig. 1. Images of the raw materials during the 24-h, 60 °C drying processes are shown in Fig. 1A and B. Fig. 1C shows the filament extrusion procedure, and Fig. 1D displays the real-time monitoring of the filament diameter. The filaments were positioned in drying for 24 h at 60 °C to eliminate any remaining moisture (Fig. 1E). As shown in Fig. 1F, dried filaments were used in the 3D printing method. Next, the printed samples were subjected to structural analysis and mechanical testing, as shown in Fig. 1G and H, respectively. SEM, EDS, TGA, DSC, Raman, rheological tests, and AFM were carried out to fully characterize the prepared composites and evaluate the effect of the addition of WC on the overall response of ABS in MEX 3D printing. Before their use for the preparation of the composites, the WC nanoparticles (NPs) were examined for their geometrical characteristics (size and shape) using SEM, while EDS was used to verify their compositional structure. The processes are presented in the supplementary material.

2.1. Materials

Detailed information on the investigated materials is provided in the Supplementary Information. Initially, SEM/EDS was used to resample the elemental composition prior to its addition to the polymeric matrix. The analysis was conducted with the aid of a field emission SEM, JSM/IT700HR manufactured by Jeol (Tokyo, Japan). The EDS measurements used to establish the chemical composition are shown in Fig. 2. Fig. 2A presents the WC powder utilized in the study, while Fig. 2B demonstrates the precise weighing of WC powder to ensure an accurate concentration of the compounds. A two-step extrusion process was used to prepare the nanocomposites. Initially, filaments were produced using a Noztek extruder (Noztek, Shoreham by Sea, United Kingdom). A shredder from 3devo (Utrecht, Netherlands) was used to turn the filaments into pellets. The extruder 3devo Composer (Utrecht, the Netherlands) employed in this work, featuring a specially engineered screw for mixing and melting materials, was used to produce filaments compatible with the 3D MEX printing process. The extruder's first zone had a temperature of 220 °C, the second and third heating zones had temperatures of 230 °C, and the fourth was set at 240 °C. The fan speed was adjusted to 55%, and the turning speed of the screw was set to 3.5 rpm, to support filament cooling during the manufacturing process. Finally, 1.75 mm diameter nanocomposite filaments were created for each WC concentration. The two above-mentioned extrusion techniques were applied to enhance the spreading of WC particles within the polymeric matrix. Pure ABS filaments were produced using the same procedure and utilized as a reference for assessing the mechanical characteristics of the nanocomposites. Fig. 2C highlights the detection of

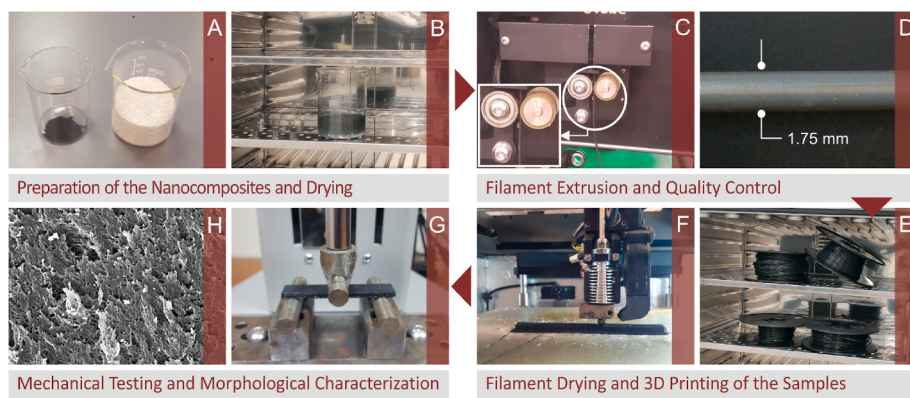


Fig. 1. Flow diagram presenting the experimental strategy employed, along with accompanying images that provide a clear visual representation of each distinct process step.

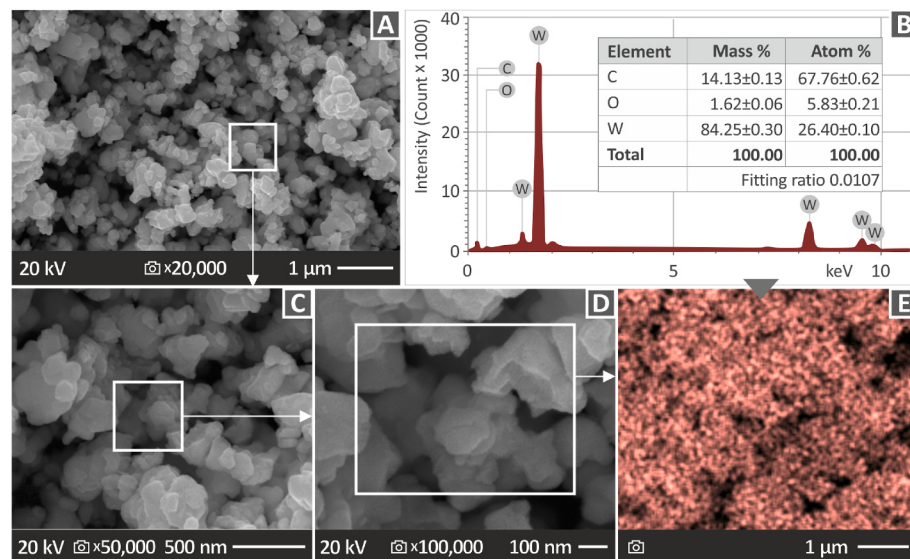


Fig. 2. The study of WC powder in the SEM apparatus is showcased through a series of steps: (A) 20,000 × magnification, (B) Analysis of the elemental composition using an EDS graph, (C) 50,000 × magnification at the region indicated in (A), (D) 100,000 × magnification at the area denoted in (C), (F) EDS Tungsten mapping depicting a uniform dispersion of the tungsten (W) element. The WC nanopowder was procured from Nanographi in Ankara, Turkey, is 99.9% pure, and has a particle size of 150–200 nm.

carbon (C) and tungsten (W), which displayed noteworthy peaks in the EDS data. Another finding was the presence of oxygen, which constituted approximately 1.62% of the total amount, and might have originated from moisture. The EDS graph shows that the chemical composition of the WC particles is consistent with the components

mentioned in the specifications of the manufacturer. The morphology of the WC particles, as illustrated in Fig. 2D and E, was investigated using SEM analysis. The results of the tungsten (W) component in the WC particles are shown in Fig. 2F. The mapping indicates that the distribution of W is essentially uniform, with only a few minor voids or

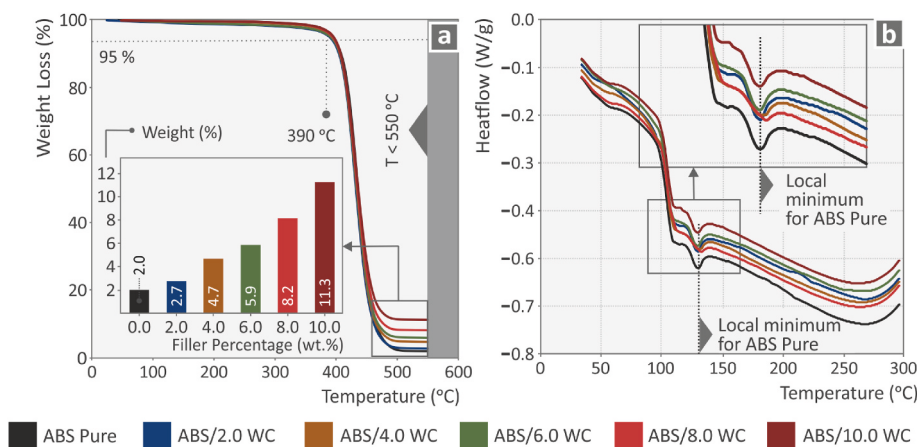


Fig. 3. Investigation of thermal behavior of Pure ABS and ABS/WC composites through (A) Weigh loss over temperature plots and (B) heat-flow plots across varied temperature ranges.

isolated places indicating variance in the W concentration. The shape and size of the NPs were verified.

3. Test results

3.1. TGA (Thermogravimetric Analysis) and DSC (Differential Scanning Calorimetry)

The mass reduction of the studied composites as well as that of the pure ABS as an expression of temperature using thermogravimetric analysis (TGA) graphs is shown in Fig. 3a. The inset bar charts represent the residual weight after the integration of the TGA procedure. These graphs show how weight changes as the temperature increases and offer valuable details about the material's thermal stability and disintegration patterns. It is apparent from the results in Fig. 3a that the incorporation of WC particles had little or no influence on the resistance of the ABS material to thermal degradation. All the composite materials experienced strong weight loss at approximately 390 °C, which was approximately the same temperature at which pure ABS began to lose weight. The residuals, as depicted by the curves at the end of the measurements, correspond to the different percentages of WC particles present in the samples. The DSC curves revealed similar behavior in terms of glass transition and crystallization temperatures. However, the addition of WC nanoparticles appeared to shift the curve to higher heat flow values, indicating higher thermal stability [39].

3.2. Analysis of rheological characteristics

Fig. 4A shows the outcomes acquired from the rheological measurements performed at 240 °C, with regard to viscosity and stress in correlation with the shear rate, displayed on the logarithmic axes. The addition of WC nanoparticles did not alter the rheological profiles of the samples, except for the sample containing 2.0% WC. The results showed that for each composite, the viscosity generally decreased with increasing shear rate. At low shear rates, the specimens revealed a quasi-Newtonian region with a small variance in viscosity, which was approximately 10⁵ Pa s. Under higher shear stresses, all the specimens exhibited non-Newtonian shear-thinning performance.

Fig. 5B displays the outcomes acquired from the MFR tests at 230 °C, that is, MFR (in g/10.0 min) versus nanofiller loading. In general, the flow rate improved with the incorporation of additives compared to pure ABS, with the greatest value measured at an additive loading of 2 wt %. A greater loading gradually reduced the compound material flow rate.

3.3. Raman spectroscopy

As shown in Fig. 5A, the Raman spectra were derived mainly from pure ABS. No clear Raman spectral differences were observed that could

be attributed to the WC additive, except for two small changes that were close to the noise level. The first difference was an increase at 1032 cm⁻¹ (C-C and C-O vibration), the second was an increase between 2900 and 2950 cm⁻¹ (C-H vibration), and the last increase was at 3065 cm⁻¹ (O-H stretching). All differences showed a gradual increase with the percentage of WC additive used. Table 1 presents the associated Raman peaks from the pure ABS sample, which is supported by the literature.

3.4. Performance of the filaments

To ensure consistent and repeatable filament quality, the closed-loop mechanism integrated into the extrusion machine used (3devo composer) was used to precisely monitor the filament diameter throughout the extrusion operation. Two randomly chosen samples of the filaments produced are shown in Fig. 6A and B. A KERN & SOHN GmbH optical stereoscope (Albstadt, Germany) was used to capture the images. These photographs were taken to visually inspect and thoroughly analyze the traits and quality of the filaments. Fig. 6A shows the pure ABS filament, while Fig. 6B shows the ABS/WC 6.0 wt % filament (nanocomposite which contains 6.0 wt percent of WC - tungsten carbide additive). Both filaments exhibited smooth surfaces without any observable flaws or defects. The figures additionally demonstrate the real-time monitoring of the filament diameter for both ABS/WC 6.0 wt % composite and the pure ABS filament. The data analysis revealed a small deviation of approximately 200 µm in the filament diameter measurements. Within the framework of MEX 3D printing, this deviation was considered acceptable. Therefore, the suitability of the experimental methods used and the precise choice of controlled variables throughout the experimental procedure were verified.

Fig. 6C shows the results of the filament tensile test. The results showed that, except for the ABS/WC 10.0 wt % filament, the tensile strength increased for all concentrations of WC. The tensile strength of ABS/WC is 10.0 wt % filament was slightly lower than for the pure ABS filament. A filament containing 4.0 wt % WC showed the most notable improvement in tensile strength when measured against the pure ABS sample, with an increase of up to 28.6%.

Fig. 6D shows how the WC additive affected the stiffness of the filaments that were created. The addition of WC particles changed the stiffness for all filament samples, excluding ABS/WC 10.0 wt % filament, which showed a decline in stiffness. The ABS/WC 4.0 wt % compound showed the greatest improvement in stiffness among all the specimens, with an increase of 19.1% in comparison to the ABS matrix. The inferior properties of the 10 wt % WC-loaded filament indicates a possible saturation of the WC additive in the ABS matrix.

The lateral surfaces of all generated filaments were examined via AFM. According to the results shown in Fig. 7, most filaments had similar surface roughness values (pure ABS and nanocomposites). However, all three surface roughness factors, Rq, Ra, and Rz, showed a

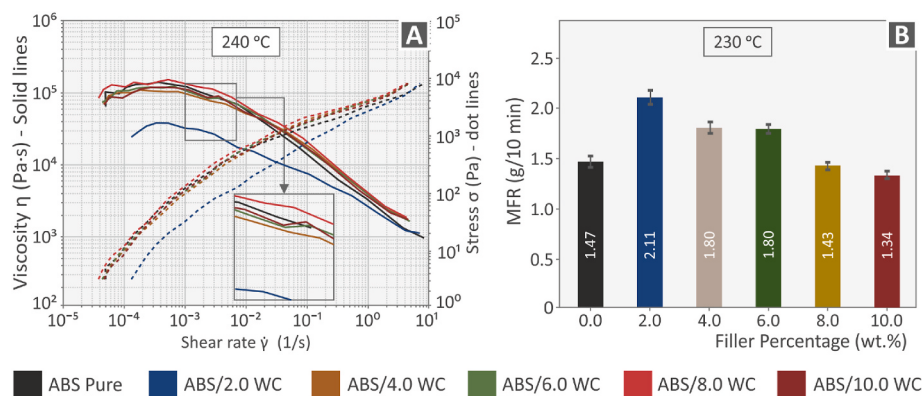


Fig. 4. Rheological analysis of Pure ABS and ABS/WC Compounds: (A) Relationship between viscosity and stress with shear rate, and (B) MFR concerning additive percentage.

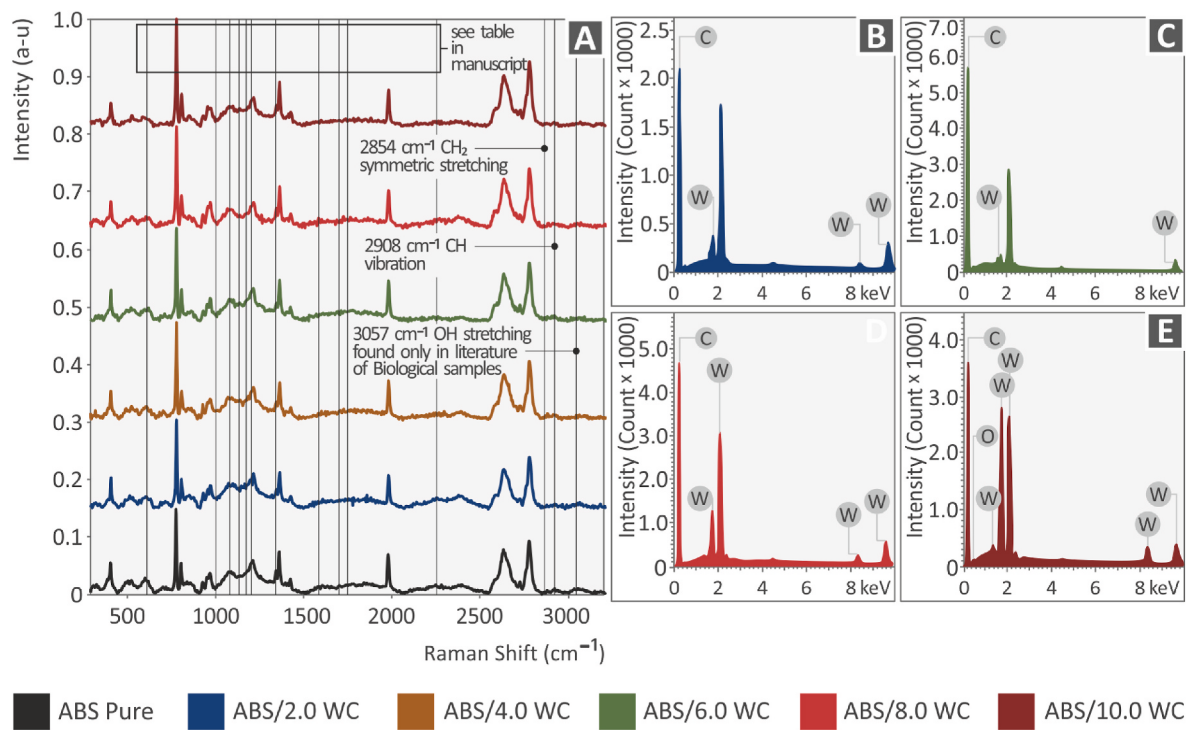


Fig. 5. (A) Raman spectra. EDS investigation for ABS/WC composites: (B) ABS/2 WC, (C) ABS/4 WC, (D) ABS/8 WC, (E) ABS/10 WC.

Table 1
Identification and assignment of the main Raman peaks observed in pure ABS.

Wavenumber (cm ⁻¹)	Raman peak assignment
618	C-C twisting found only in the literature on biological specimens [40]
1000	C-H in-plane bending [41]
1029	C-C and C-O vibration [42]
1153	Antisymmetric Si-O- stretch [43]
1178	C-O-C stretching [41]
1194	C-O-C stretching [44]
1447	CH ₃ bending [41,44–46]
1578	Raman spectrum bands of Carbon C-C stretching [47]
1600	Skeletal vibration of the C=C aromatic ring [48,49]
1663	C=O symmetric vibration found only in the literature of biological samples [40]
2234	C≡N stretching vibrations found only in the literature of biological samples [40]
2854	CH ₂ symmetric stretching [42]
2908	CH vibration [42]
3057	OH stretching found only in the literature of biological samples [40]

significant increase in the filament with the highest concentration of WC particles (10.0 wt %). Fig. 7G–I shows the relationship between the concentration of WC in the compounds and roughness metrics, including R_q, R_a, and R_z. It should be noted that the surface roughness is not solely affected by the presence of nanoparticles on the surface of the filament or is caused by possible agglomeration. It is a metric that affects material flow, and the filament clogs the nozzle. The surface roughness provides a qualitative indication of the quality of the filament produced. Filament quality is related to the processability of the MEX 3D printing process. Low-quality filaments with rough surfaces can cause problems in the MEX 3D printing process [50]. Additionally, the surface roughness metrics were calculated by statistical measurements in the region of measurement, and The R_a and R_q surface roughness values provide a statistical metric for the surface roughness in the measurement area; therefore, the highest peaks and lowest valleys are not always

considered in these metrics. The R_z surface roughness metric showed deviations from the average line of the surface. From the AFM measurements, it can be observed that the R_z value constantly increases with an increase in the WC nanoparticle loading in the nanocomposites. Therefore, a constant pattern is observed. At a maximum loading of 10 wt %, the R_z metric triples its value compared to the previous loading of 8 wt % which is a significant increase, indicating a notable change in the nanocomposites. The 2 wt % nanocomposite had an R_z value of 645.7 nm, while the corresponding value for the 8 wt % nanocomposite was 772.5 nm. This represents an almost 17% increase in the R_z value.

3.5. Mechanical assessment of 3D-Printed specimens

After analysis of the filaments, tensile tests were performed in accordance with ASTM D638-02a guidelines to determine the mechanical performance of the 3D-printed samples. The graphs in Fig. 8A show how the estimated strain (mm/mm) and tensile stress (MPa) are related to one another. The mean tensile strength (in MPa) at the point at which failure occurred for each material is shown on the Y-axis in Fig. 8B, while the X-axis represents the filler weight-to-weight percentage. These findings revealed the 3D-printed samples' tension-related mechanical properties of strength. For each examined filler percentage, as well as for pure ABS, the tensile modulus of elasticity measured in MPa is shown in Fig. 8C. This graph illustrates the stiffness or rigidity of both pure ABS and ABS compounds at different WC filler contents. According to the test results, all the samples with different WC filler concentrations outperformed the pure ABS in terms of tensile qualities, with the exception of the sample with the highest WC filler concentration (10.0 wt %), which showed a decline. Notable improvements in the tensile strength (29.4%) and stiffness (32.2%) were observed in the sample with 4.0 wt % WC. These results suggest that the capacity of the compounds to improve their tensile properties was restricted, with the highest values obtained for the sample containing 4.0 wt % WC. Above this concentration, the properties of the samples did not improve significantly. This suggests that a saturation point had been reached for the tensile characteristics of the compounds at this WC loading.

Subsequently, compression experiments were conducted in

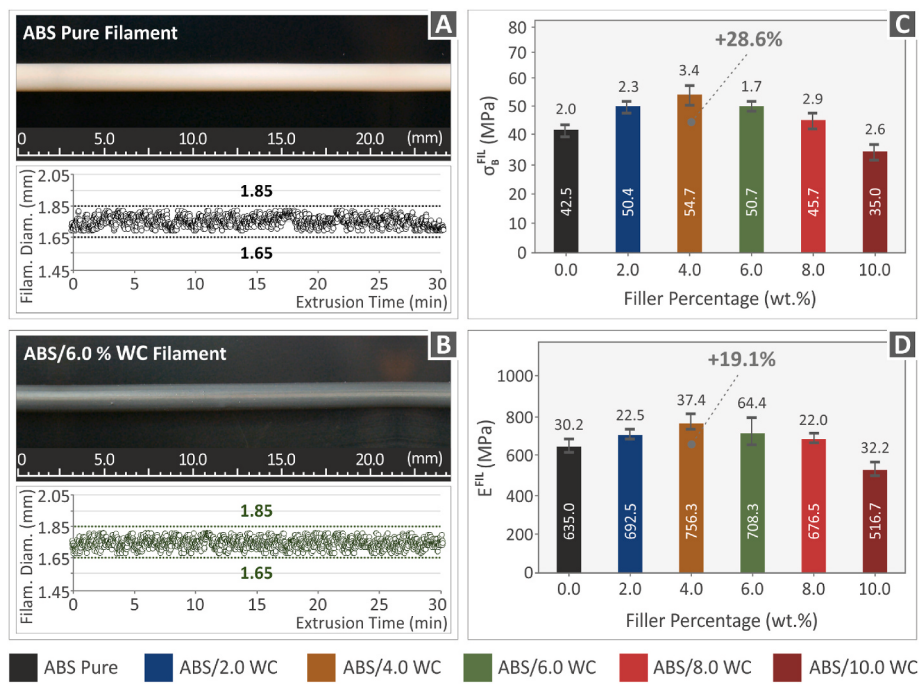


Fig. 6. Real-time monitoring of extruded filament segments for two filament types: (A) pure ABS, (B) ABS/6.0 WC, (C) σ_B^{FIL} , (D) E^{FIL} .

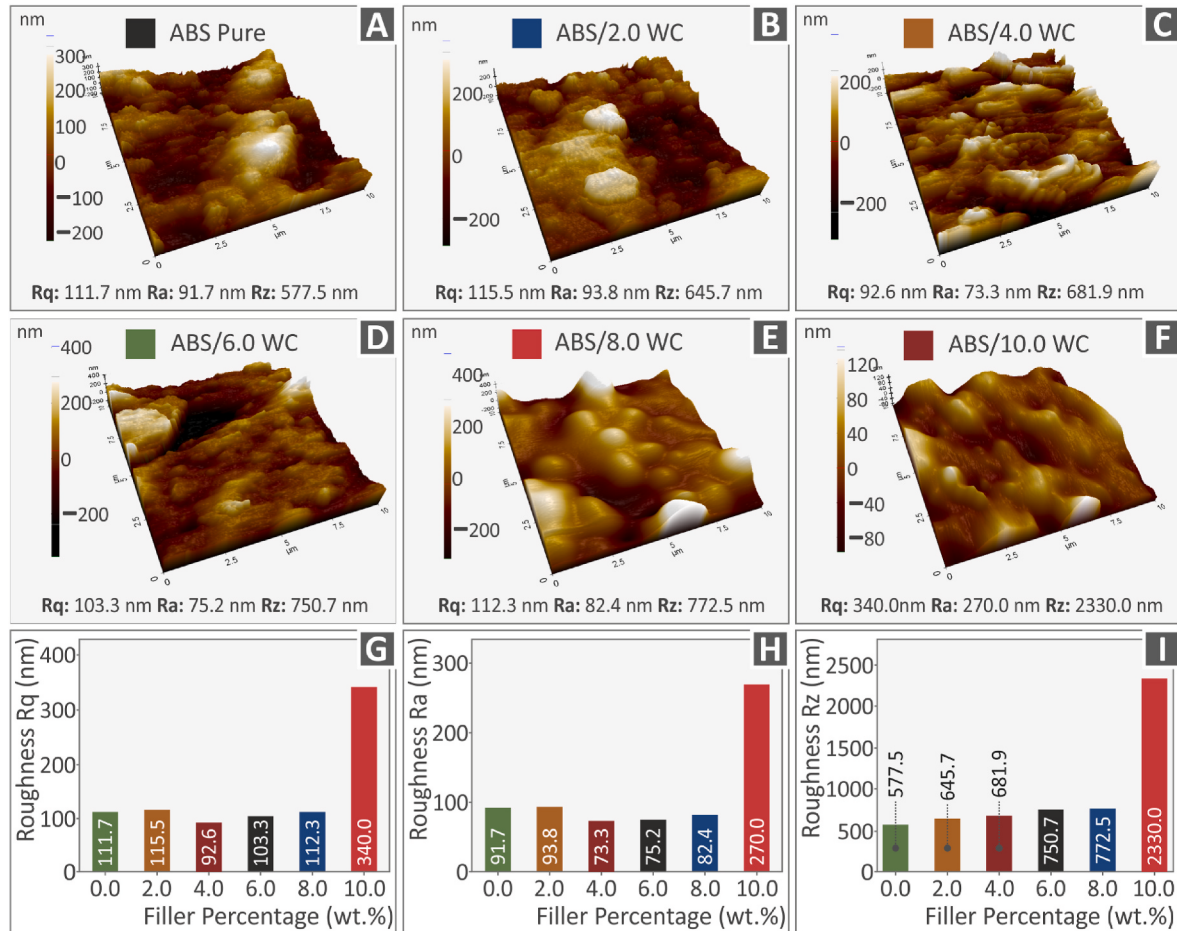


Fig. 7. AFM photos of the lateral surfaces of the examined filaments: (A) virgin ABS, (B) ABS/2.0 WC, (C) ABS/4 WC, (D) ABS/6 WC, (E) ABS/8 WC, and (F) ABS/10 WC. Graphs illustrating the correlation between WC concentration and filament roughness factors in the compounds: (G) Rq, (H) Ra, and (I) Rz.

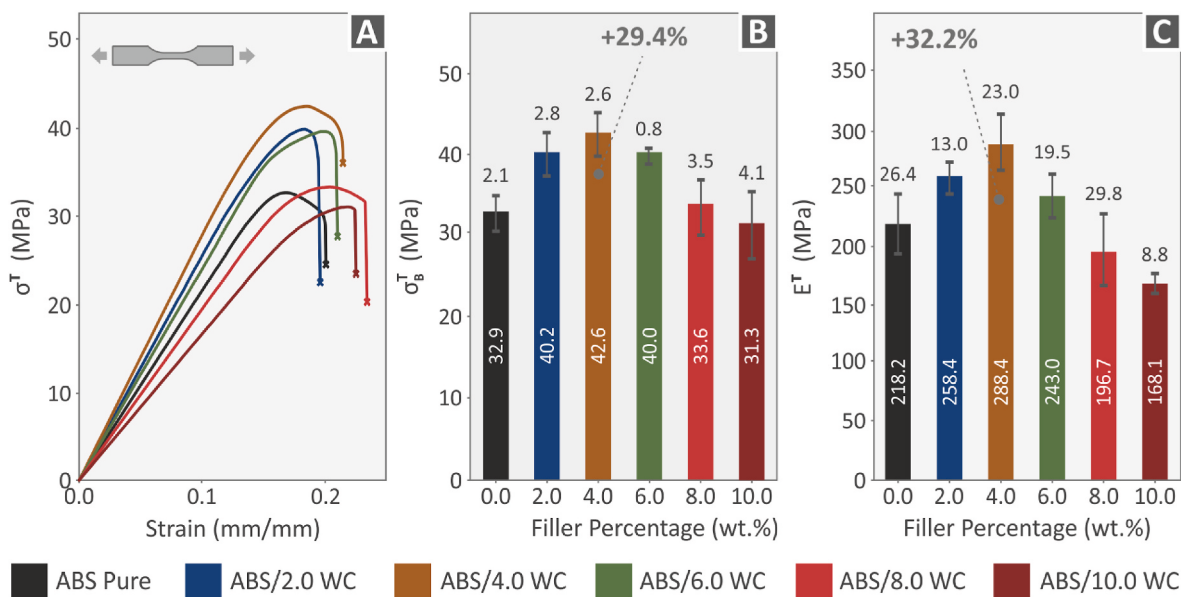


Fig. 8. Results from the tensile testing of the 3D-printed specimens: (A) Representative graphs demonstrating the correlation between tensile stress and strain for samples chosen at random from each nanocomposite material, (B) Mean values of the tensile strength, and (C) Mean values of the tensile modulus of elasticity.

accordance with the ASTM D695 guidelines. It was decided that the experiments should be terminated at a 15% maximum strain for the testing because no valuable information is expected beyond this point for the performance of the samples under compressive loading. A summary of the compression test result analysis performed on specimens made of ABS/WC composites and ABS in pure form is shown in Fig. 9. The stress-strain graphs for the tested samples under compression are shown in Fig. 9A, which depicts the connection between the applied stress and the resulting strain. Fig. 9B shows the average compression strength of the samples, which represents the highest stress that the materials can withstand when compressed. The 3D-printed samples' typical compression modulus of elasticity is shown in Fig. 9C, which provides details on the resistance of the material to deformation under compression. According to the results of the compression experiment, all

composites exhibited greater compression strength than pure ABS, as shown in Fig. 9B. A substantial improvement of 20.9%, when compared to pure ABS was observed at a concentration of 4.0 wt %. The 4.0 wt % WC composite also showed the most noticeable improvement in the compression modulus of elasticity, as seen in Fig. 9C, with an increase of 20.4% over the pure ABS material. The results showed that when compared to all other compositions tested, the inclusion of WC fillers at a concentration of 4.0 wt % resulted in the most significant improvement in compression strength and modulus of elasticity.

Moreover, Fig. 10 provides an analysis of the flexural characteristics of samples made of pure ABS and ABS/WC composites. The stress-strain curves are shown in Fig. 10A. Fig. 10B illustrates the typical flexural strength values, whereas Fig. 10C presents the typical flexural modulus of elasticity observed in the 3D-printed objects. These findings provide

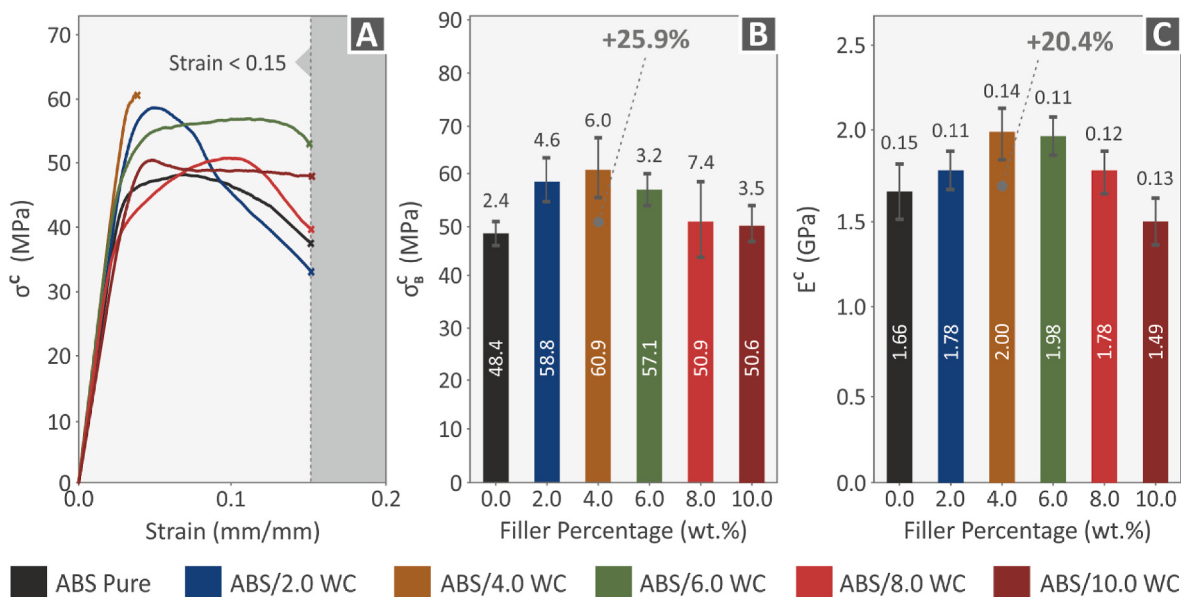


Fig. 9. Compression experiments conducted on all the 3D-printed specimens. (A) Graphs demonstrating the relationship between compression stress and the calculated strain for a specimen chosen at random from each nanocomposite, representing one of the five printed specimens. (B) Average values and standard deviations of σ_B^C (C) Average outcomes of the compression modulus of elasticity.

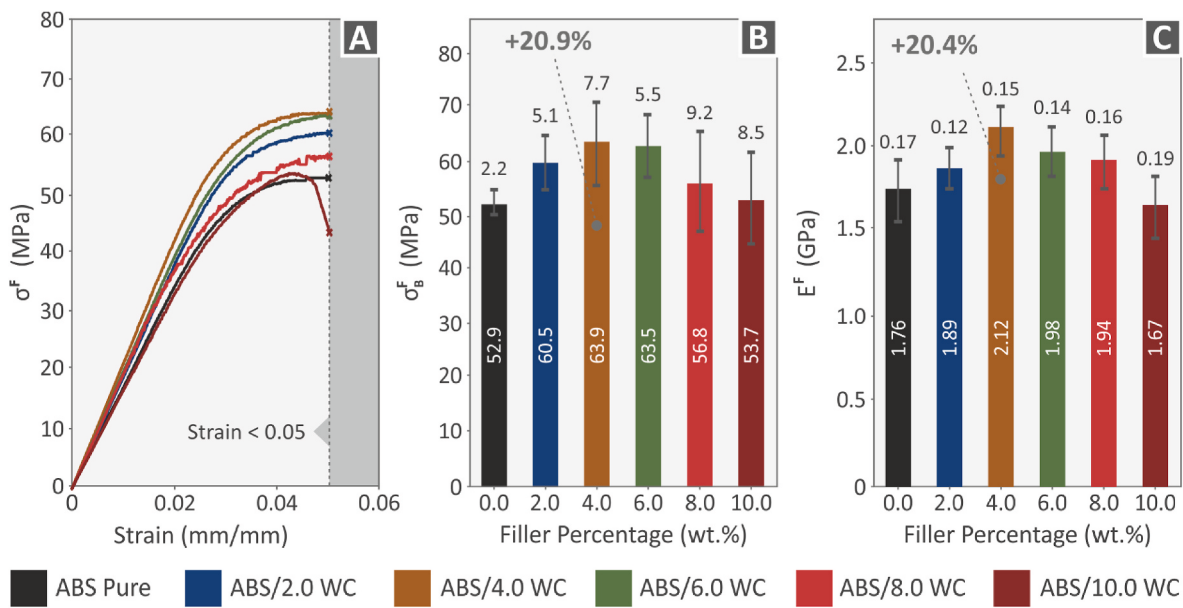


Fig. 10. The outcomes of the flexural tests conducted on all the 3D-printed specimens. (A) Graphs demonstrating the stress-strain curves for flexural strength, representing randomly selected specimens from each composite, (B) Typical values and standard deviations of σ_B^F , (C) Typical values and standard deviations of E^F .

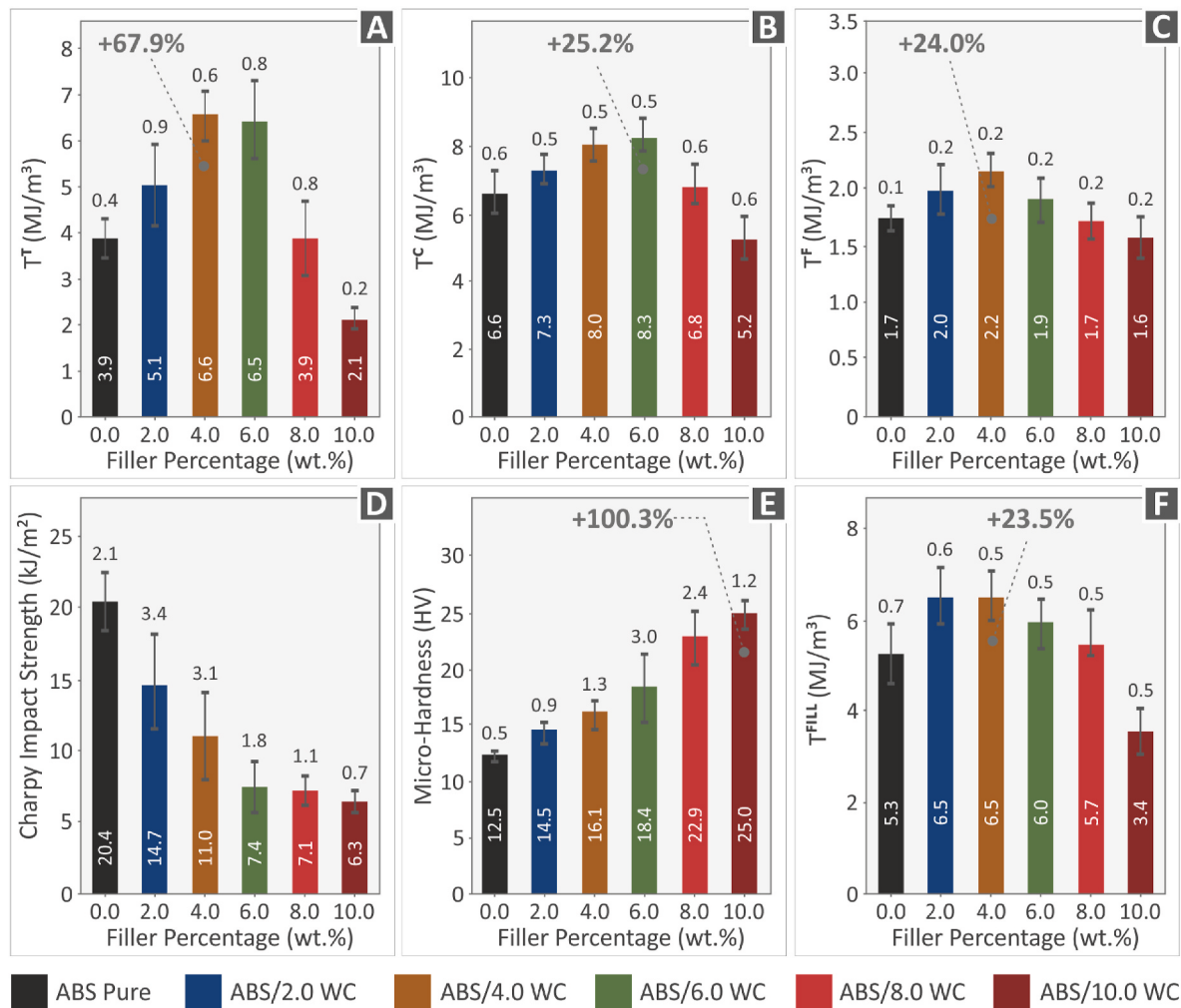


Fig. 11. The typical values and standard deviations of various mechanical properties were analyzed for both the fabricated specimens and filaments: (A) Tensile toughness of the fabricated specimens, (B) Compression toughness of the created samples, (C) Flexural toughness of the created samples, (D) Impact strength, (E) Vickers micro-hardness values, (F) Tensile fill strength of the created filaments.

insights into the resistance of materials to bending and stiffness under flexural loading conditions. It is important to note that the ASTM D790-10 standard, which specifies 5% strain as the limit for carrying out flexural testing, was followed in determining and calculating the mean values of flexural strength. Following this standard, the flexural strength of the tested samples was consistently evaluated. The flexural strength improved significantly for all the nanocomposites. The greatest improvement in flexural strength was observed for the compound with 4.0 wt % WC, which produced a maximum flexural strength. In this case, the flexural strength was higher than pure ABS by 20.9%. A composite material with a 4.0 wt % loading also displayed the highest flexural modulus of elasticity, showing a considerable rise of 20.4% compared to pure ABS.

Mechanical testing of the prepared nanocompounds, both in filament and specimen form, yielded measurements of toughness, which are shown in Fig. 11A–C and F. The stress–strain graphs were used to calculate the amount of energy that was absorbed during the testing

procedure. The tensile, compression, and flexural toughness values were calculated by integrating the relevant stress-strain curves. These results provide information on the capacity of the materials for energy absorption and deformation under different types of loads. The tensile toughness of the investigated specimens increased, as shown in Fig. 11A, with the maximum value obtained at a WC filler concentration of 4.0 wt % and representing a 67.9% improvement over pure ABS. In contrast to pure ABS, the sample with 10 wt % WC filler showed a lower value, as expected by its performance in the tests. The same pattern emerged for the tensile toughness of the filaments, where the compound with a 4.0 wt % concentration showed the highest value with a 23.5% increase and the compound with a 10.0 wt % concentration showed the lowest value (Fig. 11F). The maximum compression toughness was found at a 6.0 wt % concentration, representing a 25.2% increase (Fig. 11B). The sample with the highest filler concentration (10.0 wt %) was also the only one to show a drop in compression toughness. Similar to what was observed in previous toughness tests, the flexural toughness showed the same

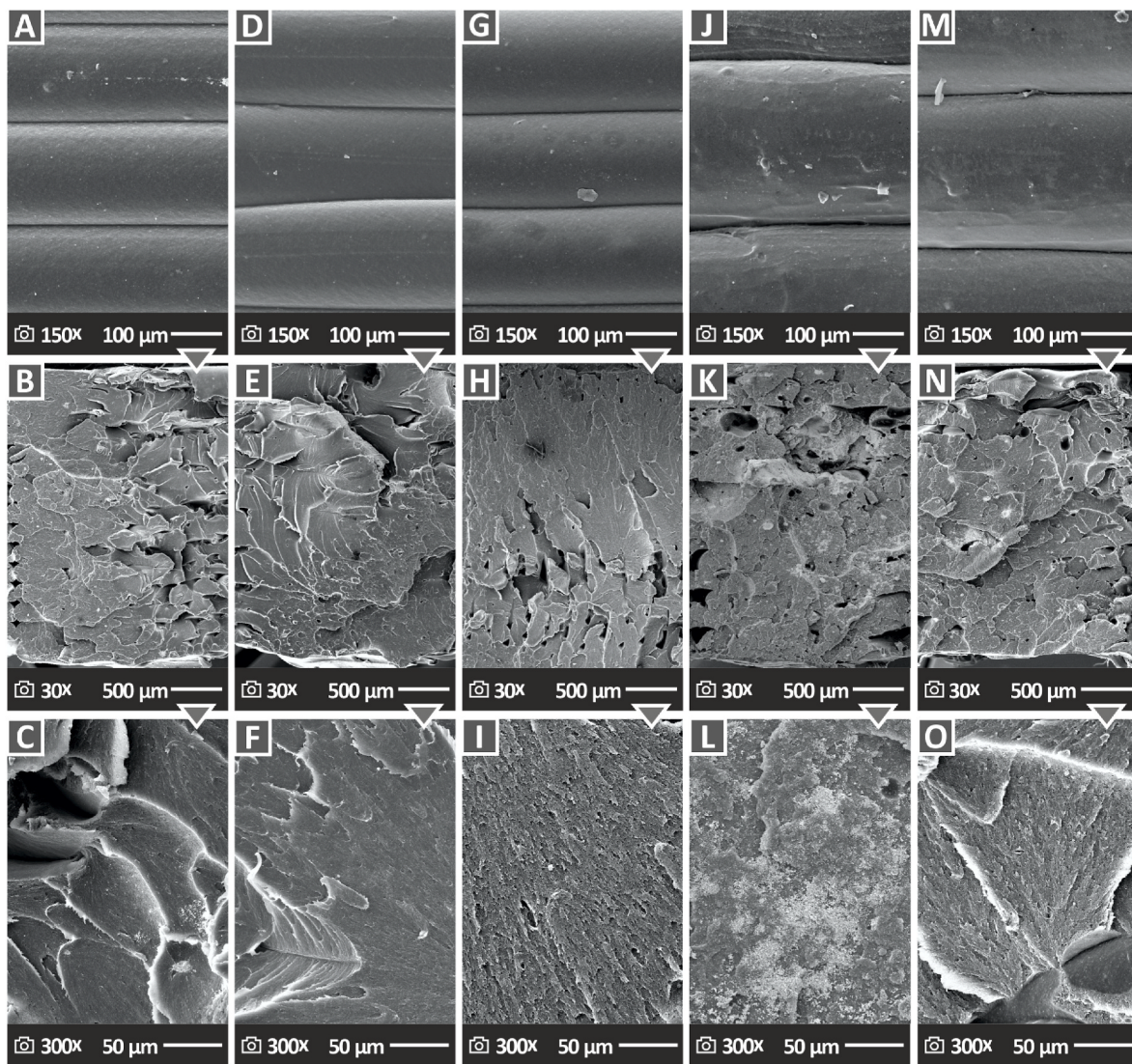


Fig. 12. A series of SEM images showcasing different magnifications and surfaces of the specimens: (A) Side surface of ABS/WC 2.0 wt% sample at an enlargement of $150 \times$, (B) Fracture surface of ABS/WC 2.0 wt% sample at an enlargement of $30 \times$, (C) Fracture surface of ABS/WC 2.0 wt% sample at an enlargement of $300 \times$, (D) Side surface of ABS/WC 4.0 wt% sample at an enlargement of $150 \times$, (E) Fracture surface of ABS/WC 4.0 wt% sample at an enlargement of $30 \times$, (F) Fracture surface of ABS/WC 4.0 wt% sample at an enlargement of $300 \times$, (G) Side surface of ABS/WC 6.0 wt% sample at an enlargement of $150 \times$, (H) Fracture surface of ABS/WC 6.0 wt% sample at an enlargement of $30 \times$, (I) Fracture surface of ABS/WC 6.0 wt% sample at an enlargement of $300 \times$, (J) Side surface of ABS/WC 8.0 wt% sample at an enlargement of $150 \times$, (K) Fracture surface of ABS/WC 8.0 wt% sample at an enlargement of $30 \times$, (L) Fracture surface of ABS/WC 8.0 wt% sample at an enlargement of $300 \times$, (M) Side surface of ABS/WC 10.0 wt% sample at an enlargement of $150 \times$, (N) Fracture surface of ABS/WC 10.0 wt% sample at an enlargement of $30 \times$, (O) Fracture surface of ABS/WC 10.0 wt% sample at an enlargement of $300 \times$.

pattern. The maximum value obtained for ABS/WC 4.0 wt % sample presented a considerable increase of 24.0% over pure ABS. As opposed to the pure ABS material, the sample with a 10.0 wt % filler content showed a lower level of flexural toughness. These results demonstrate a general pattern of increased toughness up to a particular concentration of WC filler (4.0 wt %) and a subsequent decline at higher concentrations (10.0 wt %).

The outcomes of the impact experiments are shown in Fig. 11D, and the results of the Vickers microhardness tests are shown in Fig. 11E. To account for the different filler concentrations, the mean Charpy impact strength (measured in kJ/m^2) and Vickers microhardness (measured in HV) were analyzed for all the materials examined. These measurements revealed information about the impact resistance and hardness properties of the materials at various filler concentrations. The impact strength decreases linearly with increasing filler concentration, as shown in Fig. 11D. Fig. 11E, on the other hand, showed a linear and progressive increase in microhardness as the filler concentration increased. The microhardness achieved a value of 25.0 HV, which was 100.3% greater than that of unfilled ABS, at the highest concentration of 10.0 wt %. According to these results, the materials exhibited a decreased impact strength but improved hardness as the filler concentration increased.

3.6. Morphological classification of the 3D-Printed specimens

The fractured and lateral surfaces of the 3D-printed specimens were carefully inspected by SEM. This method provides an in-depth picture of the morphology of the specimens, enabling thorough observation and

analysis of their surface properties. The SEM images of the lateral surfaces of the 3D-printed samples are shown in Fig. 12A, D, G, J, and M. The samples represented by these photographs are ABS/WC composites with the following weight percentages: 2 wt %, 4 wt %, 6 wt %, 8 wt %, and 10 wt %. To facilitate a thorough examination of the morphological properties of the samples, the lateral aspects of each one were 150 times magnified. The interconnections between the layers were devoid of flaws and cavities, according to the SEM images of the examined samples. Except for the specimen with an 8.0 wt % filler loading, which displayed uneven layer morphologies, the photos showed that the layer structure was constant for the majority of samples. This outcome indicates that 3D printing was appropriate, and the quality characteristics did not negatively affect the mechanical performance.

The fracture surfaces of randomly selected tensile samples are depicted in Fig. 12B, E, H, K, and N at $30 \times$ magnification and in Fig. 12C, F, I, L, and O at $300 \times$ magnification. All the specimens in the figures reveal microvoids and microporosity at a magnification of $30 \times$, particularly close to the edges of the specimens. Regardless of the 100% infill ratio utilized, these microvoids have previously been reported in the literature for the structure of 3D-printed objects and are frequently present because of the layer-by-layer building technique used in MEX 3D printing [13]. The studied samples exhibited a more ductile fracture mechanism when inspected closely at a magnification of $300 \times$. This suggests that more plastic deformation occurred in the materials. However, the samples with higher and lower filler concentrations exhibited more pronounced distortions in their fracture surfaces. This can be observed in Fig. 12C and O, where the distortion appears to be

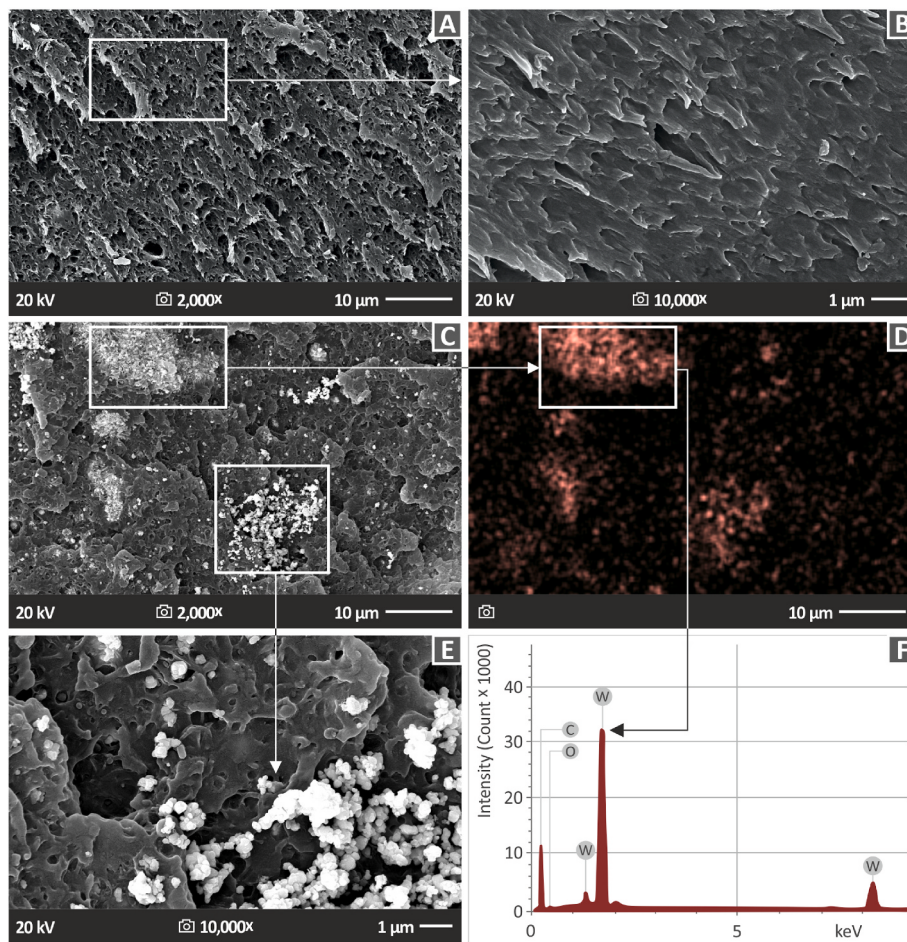


Fig. 13. SEM pictures demonstrating: (A) ABS/WC 4.0% at $2000 \times$ exaggeration, (B) ABS/WC 4.0% at $10,000 \times$ exaggeration, (C) ABS/WC 10.0% at $2000 \times$ exaggeration, (D) EDS map for the W component, (E) ABS/WC 10.0% at $10,000 \times$ exaggeration, and (F) EDS for the ABS/WC 10.0% obtained from a region rich in WC particles.

more pronounced compared to the other samples.

Fig. 13 presents the SEM images of the agglomerations of particles present in the samples. In **Fig. 13A**, an SEM photo at $2000 \times$ magnification shows that the ABS/WC 4 wt % composite. No agglomerations are observed in the image. To provide further insight, **Fig. 13B** shows a higher magnification ($10,000 \times$) of the same area, as shown in **Fig. 13A**. In **Fig. 13C**, an SEM photo at $2000 \times$ magnification shows that the ABS/WC 10 wt % composite, revealing the presence of clustered WC particles, indicating a non-uniform distribution. To provide further insight, **Fig. 13E** shows a higher magnification ($10,000 \times$) for the same area, as shown in **Fig. 13C**. This close-up view exposes the microporosity on the surface along with the clustered WC particles. Additionally, **Fig. 13D** presents an EDS map of the region observed in **Fig. 13C**, specifically highlighting the distribution of tungsten. The distribution of W in **Fig. 13D**'s EDS mapping supported the conclusion that the particles shown in **Fig. 13C** were, in fact, WC particles. Furthermore, the agglomeration zone within the 10 wt % filler loading is displayed by the EDS graph in **Fig. 13F**. The graph shows a clear peak for tungsten (W), indicating that this element is highly concentrated in the area being studied. These findings partially justify the reduced mechanical behavior of the specimens made with nanocompounds of this concentration (10 wt %), since NPs agglomerations negatively influence the mechanical properties of the samples [51]. At lower WC-loaded nanocomposites, no agglomerations were observed during the SEM observations, as shown in **Fig. 13A** and B.

4. Discussion

A summary of the mechanical experiments conducted on both the compounds under investigation and the pure ABS material is shown in a spider graph form in the supplementary material. In general, the incorporation of WC particles enhances the material characteristics of pure ABS; therefore, the hypothesis of this study was confirmed. WC NPs reinforced the ABS polymeric matrix for MEX 3D printing. Additionally, an impressive improvement was achieved in the microhardness measurements, making the nanocomposites compatible with applications with such specifications. It should be noted that the highest microhardness was achieved with the 10 wt %, which did not perform as well in the remaining mechanical tests. Therefore, according to the requirements of each application, the loading of the WC NPs can be adjusted to either achieve improved mechanical properties in most tests or to achieve extremely high polymer microhardness performance, which, as mentioned, indicates nanocomposites with high wear resistance. It was concluded that the chemical reactions occurring at the interface between the ABS matrix and WC particles may have improved the mechanical properties. These results underlined the significance of the relationship between the filler and matrix, as well as the contribution of chemical processes in improving the mechanical performance of composite materials [35].

In this study, the amount of WC additive was gradually increased and mechanical tests were conducted for each loading. As long as the response was maintained at high levels and higher than that of pure ABS, the WC was further increased, and the experiments were repeated. In this way, the maximum loading of WC nanoparticles in the ABS matrix, using the specific nanocomposite preparation method, was estimated. When the mechanical properties were lower than those of pure ABS, the process was terminated, indicating that the saturation point was around the specific loading. Therefore, this experimental process was followed to estimate the best mechanical properties that could be achieved with the specific additive in the specific matrix by the methodology followed. The loadings could be considered high for the nanoadditives. This was also verified by the experimental procedure in which 4 wt % loading achieved the best mechanical performance among the loadings tested. Furthermore, loadings up to 15 wt % are reported in the literature for nanoparticles in the nanocomposites [52,53].

A composite with a loading of 4.0 wt % displayed the greatest

mechanical performance in most tests among the several compounds synthesized and evaluated in this investigation, demonstrating a clear association between the advancement of mechanical characteristics and the concentration of WC filler. This result indicated that, among the evaluated compounds, the 4.0 wt % loading was the optimal choice among the tested samples. In terms of the tensile, flexural, and compression properties, the specimens containing ABS/WC with 4 wt % loading showed the greatest improvement, with a single exception of compression toughness, where the composite with a 6.0 wt % WC filler displayed the best performance. The mechanical characteristics started to deteriorate as the WC filler concentration was raised over the 4.0 wt % loading. This suggests that higher concentrations of WC in the ABS matrix are expected to reach a saturation point. Identification of the exact saturation point was outside the scope of this investigation. By observing the spider graph in the supplementary material of the study, which summarizes the mechanical test results, it was shown that the 4 wt % has superior performance in all the mechanical properties, except the impact strength and the microhardness. Therefore, it is considered to be the best option for its performance, as mentioned above. This can be attributed to the formation of an optimum nanoparticle network among the loadings studied. By inspecting the rheological results, it was shown that the specific loading had a similar viscosity to the remaining loadings, with only 2 wt % loading having a lower viscosity. Its MFR was also the second highest after 2 wt % loading. This indicates good processability behavior, forming a good quality 3D printed structure, which also contributes to the superior performance of the 4 wt % nanocomposite. At higher concentrations, the mechanical properties start to decrease, as do the MFR values, again verifying the connection between the mechanical properties and rheological characteristics, which affect the processability of the nanocomposites in the 3D printing process. The decrease in MFR can again be attributed to the increase in nanoparticle loading, which probably indicates non-homogeneous dispersion in the nanocomposites, along with the different interactions between the nanoparticles and the matrix. It should be noted that the method followed is a thermomechanical method without any chemical reactions for the formation of nanocomposites or the fabrication of parts. So, the 4 wt % nanocomposite is considered the best option among the ones studied for the specific manufacturing method followed in the study. By inspecting **Fig. 8** (tensile test results) and **Fig. 9** (flexural test results), it can be observed that the 4 wt % sample failed at a very small elongation. A very small elongation at failure indicates a more brittle failure of the sample. It is expected that as the material becomes stiffer and has higher mechanical strength, the brittleness increases, as shown in the stress vs. strain graphs. In the reinforcement of materials, the increase in stiffness and mechanical strength are the desired outcomes, whereas the developed strain is usually not the first priority. The toughness, which indicates the energy absorbed by the sample during the experiment, is also an additional metric for the response of the material. In real-life applications, the parts are designed to operate within an elastic region without high deformations. The elongation of the samples during the tests was affected by various factors. It should be noted that in the graphs (**Fig. 8**, tensile test results; **Fig. 9**, flexural test results), one of the five samples of each nanocompound is presented. Therefore, the very small elongation shown refers to the specific test sample only and not all samples of the 4 wt % batch.

As was already mentioned, the compression toughness (T^c) also showed a noticeable improvement up to a filler loading of 6.0 wt percent, reaching a value of 25.2%. The microhardness, on the other hand, showed a consistent and positive increase up to 10 wt % additive loading, reaching 100.3%, as explained above. Only the impact strength exhibited a linear reduction in the presence of WC nanoparticles. Therefore, except for the impact tests, it appears that the amount of WC positively affects the nanocomposites.

A potential explanation for the decrease in viscosity and degree of shear thinning for samples containing 2.0 wt % WC is that the addition of WC filler reduced viscosity and the degree of pseudoplastic behavior,

up until the threshold of 2.0%, while higher contents of WC increased viscosity and extent of shear thinning. It is possible that the 2% WC particles were better dispersed within the ABS matrix compared with the higher filler loadings. Improved dispersion can lead to a reduction in viscosity, because the particles are more effectively lubricated by the polymer matrix, resulting in less resistance to flow. At higher filler percentages, particles are closely packed together, making particle-particle interactions predominate over matrix-particle interactions [54]. The viscosity values of the samples containing WC fillers at different shear rates were close to that of pure ABS, indicating that there was no chemical interaction between the additive and the matrix. This was encouraging for the employment of filament samples in 3D printing applications because their printing behavior can be predicted based on that of pure ABS. Additionally, shear thinning behavior is desirable for materials intended for 3D printing applications because it allows for a smooth flow from the nozzle to the print bed and retention of the extruded shape. This behavior has been previously reported in the literature for both pure ABS and ABS-based composites [54–58].

It should be noted that this work focuses on the 3D printing material properties; however, the effect of the filler in the process is also of interest to the authors. Therefore, rheological experiments were conducted in this study. More specifically, as shown in Fig. 5, the addition of 2 wt % WC in the ABS matrix reduces the viscosity and increases the Melt Flow Rate. A further increase in the WC loading in the nanocomposites increases the viscosity gradually and linearly with the decrease in WC content. This behavior is expected to affect the processability of the nanocomposites during the 3D printing process, which was verified by inspecting the SEM images on the side surface of the 3D printed samples, in which, at higher WC loadings, the shape and thickness of the layers were not as uniform and constant as in the lower filler concentration samples. On the other hand, the change in viscosity indicates that the 3D printing parameters needed to be optimized for each nanocomposite to achieve the best possible performance, owing to the change in the behavior of the nanocomposites with the increase in the filler loading. In this study, the authors chose to 3D print all nanocomposites with the same 3D printing settings to obtain comparable results. Changing and optimizing the 3D printing settings would require further analysis, which was not within the scope of this study. This study aimed to evaluate the effect of WC nanoparticle loading on the mechanical performance of ABS matrices. For this evaluation, the other parameters were kept constant so that the results could be compared. The optimum 3D printing settings for pure ABS were employed in all fabricated nanocomposites. Hence, as the loading increased, the quality of the 3D printed structure was affected, as shown in the SEM images of the samples (Fig. 12). This was more obvious in the samples manufactured with higher loadings of 8 wt % and 10 wt %.

Through examination of the lateral surface microstructure of the 3D-printed samples, valuable information regarding various aspects was obtained. The printing settings and parameters were verified by evaluating critical qualities, such as the thickness of each individual layer. The presence of flaws in the samples was evaluated. By analyzing the microstructure, it was possible to acquire additional information regarding the properties of the interfaces between the 3D-printed layers, which was useful in determining the degree to which those layers were fused and bonded. When the additive concentration in the ABS polymer was increased, the SEM images showed that there was no substantial increase in the number of micro-voids on the surfaces of the 3D-printed objects. In addition, the SEM examination demonstrated that the filler particles were evenly disseminated and successfully incorporated into the matrix material. However, it should be highlighted that, in comparison to specimens with higher filler contents, specimens with 8.0 wt % ABS/WC exhibited larger micro-voids. This shows that the filler distribution or bonding within the ABS matrix may not have been ideal at the 8.0 wt % loading, resulting in the creation of bigger voids. As previously discussed, such imperfections or structural differences are expected in the parts created using the MEX 3D printing technique [35].

It should be noted that agglomeration could deteriorate mechanical performance when the particle concentration reaches a high level, as reported in the literature [59,60]. To minimize the agglomeration of the nanocomposites initially, the matrix material was milled in powder form instead of the original pellet form. The powder was mixed with the filler under high-shear conditions for a long time prior to its insertion into the extruder. The filler used was nanoscale, according to its specifications. Subsequently, a two-step extrusion process was implemented by successively employing two filament extruders. This process is presented in detail in the Supplementary Material. This approach was followed to subject the nanocompounds to additional thermomechanical mixing processes in the extruders, aiming to achieve the best possible dispersion of the particles in the matrix using the methodology described in the study. It should be mentioned that a satisfactory level of nanoparticle dispersion from micro-to-nanoscale particle networks could be achieved with single-screw extruders, similar to those employed herein, as widely documented in the corresponding literature [34]. In this work, the extruder used was a 3dvo composer extruder, which has a screw with geometry specially designed for materials and nano-additive mixing, according to the manufacturer. This is a very popular extruder in the literature for the preparation of nanocomposites, in which single-screw extruders are commonly used for filament making. This specific model has superior specifications and prices compared with other extruders. The formation of agglomeration was examined afterward in the 3D-printed samples in the high-magnification SEM images. These images were used to identify possible agglomerations on the materials and evaluate the quality of the nanofiller dispersion. By inspecting the fracture surfaces of the samples using SEM, it was found that at the highest filler concentration, agglomerations could not be avoided in the structure. This affects the mechanical properties, as mentioned in this study. In the nanocomposites with lower filler concentrations, it was not possible to locate agglomerations in the structure of the samples. This finding is in agreement with the results of the current study. The WC aggregates were located in the 10 wt % loading nanocomposites and the mechanical performance of the nanocomposites was decreased compared to lower loadings. These composites showed lower tensile strength than pure ABS, and this deterioration in the mechanical properties can be attributed to the WC aggregates in the specific samples. However, the microhardness on this loading was impressively increased, showing that if such a specification is required, such loading can be achieved in cases where the remaining mechanical properties are not a priority, as mentioned. As mentioned previously, 4 wt % loading nanocomposite showed the highest mechanical performance among the nanocompounds prepared and tested. The increase in the WC loading beyond 4 wt % started to decrease the mechanical performance of the samples. Still, they maintained a higher performance than the pure ABS, showing that the addition of the nanoparticles reinforced the ABS matrix even at loadings up to 10 wt % limit of the methodology followed, which resulted in lower mechanical performance for the ABS matrix, as mentioned. Therefore, the authors believe that at a certain amount, the nanofiller has created a nanoscale network in the polymer matrix, even if some of the nanofiller may have not been dispersed, achieving a full nanodispersion. The EDS analysis of various regions of the fracture surfaces verified the above statements. Additionally, in the mechanical tests, the deviation in the results is within acceptable limits, indicating that the nanocomposites have a similar composition in all the samples studied. In conclusion, the scope of this research was to develop nanocomposites with a process that can be easily industrially expandable instead of using other (chemical) methods. Furthermore, the two-step extrusion process followed resulted in nanocomposites with good mixing between the matrix and the additives. This is supported also by the overall findings of the work (mechanical test results and morphological investigations with SEM), in which the reinforcing trend of the prepared nanocomposites is evident. In future work, different methods can be tested and evaluated. Herein, the standard thermomechanical process for filament melt mixing was followed and implemented. It should be

noted that investigating the agglomerations with SEM, which was the method followed in the current research, is a common practice in the literature [61–63].

TGA showed that the processing temperatures utilized in the MEX procedure had no negative impact on the materials employed. This was important because it ensured that any potential material degradation caused by high temperatures would not have an adverse effect on the 3D printing technique or mechanical characteristics of the specimens made with the prepared composites. Overall, the addition of WC nanoparticles did not significantly alter the thermal stability of the ABS matrix. Various factors may have contributed to this result. The nanocomposites were prepared by a thermomechanical process, without any chemical reactions between the filler and the matrix. Any changes in thermal stability can be attributed to the interaction between the nanoparticles and matrix in their contact surfaces. The effect of these interactions is outlined in the thermal tests, as the produced curves change slightly with the increase in WC loading in the nanocomposites. It can also be assumed from the outcome of the thermal tests that the WC loadings studied were not adequate to cause thermal stability issues in the ABS matrix. As previously mentioned, any changes in the thermal behavior of the nanocomposites were investigated and reported experimentally. Furthermore, the literature reports that the addition of inorganic nanoparticles to polymeric matrices can increase the thermal stability of nanocomposites compared to pure matrices [64,65].

Based on existing information, no previous research has examined the mechanical performance of the respective composites in the literature. As a result, it was not impossible to directly compare or evaluate the work's findings with previously published research. This underlines the novelty and originality of this study because it fills a knowledge gap and offers fresh perspectives on the mechanical characteristics of the investigated composites. Tungsten carbide (WC) has been used as a reinforcing ingredient in different polymer composites in MEX 3D printing has been used. A specific study presented polytetrafluoroethylene (PTFE) composites filled with WC at various weight ratios with tungsten carbide [66]. The sample of these composites with a 20% WC filler achieved noticeable tribological and mechanical qualities. This shows that the PTFE matrix's performance in terms of friction, wear resistance, and mechanical qualities was enhanced as a result of the addition of a 20% WC filler [67]. Another study examined the tensile strength and elongation characteristics of laminated constructions using a computerized universal testing apparatus. The basalt fiber-reinforced laminate with a 6% tungsten carbide filler outperformed the other laminate combinations tested in terms of strength. The epoxy composites improved both the tensile properties and percentage of elongation with the inclusion of tungsten carbide fillers, which had a synergistic impact. This shows that the use of tungsten carbide fillers improved the mechanical characteristics of basalt fiber-reinforced laminates, making them more resilient to tensile stresses and enabling greater elongation before breakage [66]. Herein, lower WC concentrations were introduced to the ABS polymer, and the improvement in the mechanical characteristics was similar, with the reported results following a similar trend to the literature mentioned above. To provide insight into the effect of different additives in the ABS matrix in MEX 3D printing, Table 2 compares the findings presented herein with the corresponding results

from the literature. The comparison results indicate that WC managed to increase both the tensile strength and the tensile modulus of elasticity in a better way than most of the compared fillers. Both organic and inorganic fillers are presented. As shown, the inorganic fillers overall managed better results.

The cost of producing 3D-printed parts with the nanocomposites reported herein is not significantly increased by adding WC particles to the ABS polymer to increase its robustness. Compared with the price of the virgin materials utilized, the manufacturing process itself has a greater overall impact on production costs. As a result, adding WC particles to ABS polymers to increase their strength remains a viable option for 3D printing applications. For orders greater than 1000 kg, ABS raw material is offered at 0.35 €/kg. The corresponding filament produced, which is the commercial product utilized in 3D printing, costs approximately 25 euros per kilogram. This considerable price disparity shows that the manufacturing procedure itself, rather than the cost of the matrix materials, is where the majority of costs are incurred. The extrusion process, quality assurance, packing, and distribution are just a few stages that involve turning raw ABS into a high-quality filament, all of which add to the overall cost. Consequently, the price of the ABS mostly dictates the cost of the filament rather than the price of the manufacturing process. The price of ABS for laboratory-scale investigations is roughly 10.0 €/kg, which is equivalent to 0.01 €/g. This price reflects the cost of the pure ABS material used in this study. The cost of WC particles for laboratory-scale research was roughly 0.5 €/g. However, WC particles might be considerably cheaper in industrial applications because of economies of scale. The increased raw material cost for the composite with a maximum mechanical improvement of 4.0 wt % can be computed as 0.5 €/g times the weight percentage of WC (0.04). Therefore, it is predicted that adding WC particles to the ABS matrix at an ideal concentration will cost an extra 0.02 EUR/g. The total cost for laboratory-scale use, including the price of ABS raw material and the additional cost of WC particles (0.01 €/g + 0.02 €/g), is approximately 0.03 €/g. This increase in cost is not important, considering that virgin materials are not the main cost in the procedure, as explained above.

5. Conclusions

The present study investigated the novel use of Tungsten Carbide (WC) ceramic, which has not been investigated in prior literature, that is, as a reinforcing agent for ABS material in MEX 3D-printing. The main goal of this study was to examine whether adding WC ceramics could enhance the mechanical properties of ABS polymers. The study effectively demonstrated through a series of experiments that adding WC ceramic powder to the ABS matrix improved the mechanical characteristics of the ABS polymer. To fully evaluate the mechanical characteristics of the polymer when mixed with WC ceramic additions, several mechanical tests were performed on the 3D-printed samples.

The mechanical characteristics of the ABS polymer matrix were significantly enhanced by the addition of the WC ceramic particles. When Compared to pure ABS, the tensile, compression, and flexural strengths all improved noticeably, with increases of 29.4%, 25.9%, and 20.9%, respectively. flexural toughness, compression toughness, and

Table 2
Effects of several additives on the ABS matrix in MEX 3D printing.

	WC (current research)	Titanium Nitride [13]	Carbon nanotubes [26]	Silicon Nitride [68]	Bamboo [69]	Cellulose nanocrystals [70]	Rice husk [71]
ceramic	yes	yes	no	yes	No	No	no
Tensile strength reinforcement (%)	29.4	18.1	~30	25.6	–	~10	Reduction
Tensile modulus of elasticity reinforcement (%)	32.2	22.2	~19	20.2	~10%	–	Reduction
Loading that achieved optimum results (wt. %)	4	6	10	4	5	3	–
Loading range studied (wt. %)	0–10	0–8	0–10	0–10	5	3	0–15

tensile toughness also significantly increased with the addition of WC, rising by 24.0%, 25.2%, and 67.9%. Additionally, there were improvements in the tensile, compression, and flexural moduli of elasticity of 32.2%, 20.4%, and 20.4%, respectively. These enhancements were supported by mechanical testing performed in compliance with international standards. With a maximum improvement of 100.3%, the WC ceramic additive's hardness also significantly enhanced microhardness, making the prepared nanocomposites compatible with applications requiring high wear resistance from the materials.

The current research focused on the reinforcement effect of WC nanoparticles on the ABS polymer when 3D printed using the MEX process. Several additional challenges were investigated. For example, the effect of the addition of WC nanoparticles on the aging of ABS polymers could be of scientific interest. Such an investigation would require additional and extensive scientific effort, which was not within the scope of the current research. This could be a subject of future research. Future work can also focus on the industrialization of the production process and investigation of the exact point of saturation of the WC filler in the polymer matrix. By adjusting the 3D printing settings, it is possible to maximize the advantages of the composite material by optimizing the strengthening effect of the WC filler in the ABS material. The practical significance of the study's findings can be increased by addressing these issues and encouraging the use of WC-reinforced ABS composites in various industries. Future investigations in these fields will advance and widen the application of WC-based composites. Finally, the results reported herein strengthen the role and value of ceramic NPs as reinforcements in MEX 3D printing.

Funding

This study received no external funding.

Data availability

The raw/processed data required to reproduce these findings cannot be shared because of technical or time limitations.

Declaration of competing interest

The authors declare that they have no known competing financial interests or personal relationships that could have appeared to influence the work reported in this paper.

Acknowledgments

The authors would like to thank the Institute of Electronic Structure and Laser of the Foundation for Research and Technology-Hellas (IESL-FORTH) and, in particular, Ms. Aleka Manousaki for taking the SEM images presented in this work and the Photonic Phononic and Meta-Materials Laboratory for sharing the Raman Instrumentation.

Appendix A. Supplementary data

Supplementary data to this article can be found online at <https://doi.org/10.1016/j.ceramint.2023.08.144>.

References

- [1] O.B. Zgalat-Lozynskyy, O.O. Matviichuk, O.I. Tolochyn, O. V Ievdokymova, N. O. Zgalat-Lozynska, V.I. Zakiev, Polymer materials reinforced with silicon nitride particles for 3D printing, Powder Metall. Met Ceram. 59 (2021) 515–527, <https://doi.org/10.1007/s11106-021-00189-2>.
- [2] S.H. Masood, W.Q. Song, Development of new metal/polymer materials for rapid tooling using Fused deposition modelling, Mater. Des. 25 (2004) 587–594, <https://doi.org/10.1016/j.matdes.2004.02.009>.
- [3] B. Yan, K. Chen, L. An, Enhanced moderate electric field dielectric energy storage performance in (Bi0.5Na0.5)TiO3-based lead-free ceramics, Ceram. Int. 48 (2022) 37020–37026, <https://doi.org/10.1016/j.ceramint.2022.08.272>.
- [4] P. Colombo, E. Bernardo, G. Parcianello, Multifunctional advanced ceramics from preceramic polymers and nano-sized active fillers, J. Eur. Ceram. Soc. 33 (2013) 453–469, <https://doi.org/10.1016/j.jeurceramsoc.2012.10.006>.
- [5] D. Nötzel, R. Eickhoff, T. Hanemann, Fused filament fabrication of small ceramic components, Materials 11 (2018), <https://doi.org/10.3390/ma11081463>.
- [6] K.-D. Bouzakis, N. Michailidis, N. Vidakis, K. Efstratiou, T. Leyendecker, G. Erkens, R. Wenke, H.-G. Fuss, Optimization of the cutting edge radius of PVD coated inserts in milling considering film fatigue failure mechanisms, Surf. Coat. Technol. 133–134 (2000) 501–507, [https://doi.org/10.1016/S0257-8972\(00\)00971-3](https://doi.org/10.1016/S0257-8972(00)00971-3).
- [7] A. Antoniadis, N. Vidakis, N. Bilalis, Fatigue fracture investigation of cemented carbide tools in gear hobbing, Part 2: the effect of cutting parameters on the level of tool stresses—a quantitative parametric analysis, J. Manuf. Sci. Eng. 124 (2002) 792–798, <https://doi.org/10.1115/1.1511173>.
- [8] K. Ravikumar, K. Kiran, V.S. Sreebalaji, Characterization of mechanical properties of aluminium/tungsten carbide composites, Measurement 102 (2017) 142–149, <https://doi.org/10.1016/j.measurement.2017.01.045>.
- [9] I.C. Visconti, A. Langella, M. Durante, The wear behaviour of composite materials with epoxy matrix filled with hard powder, Appl. Compos. Mater. 8 (2001) 179–189, <https://doi.org/10.1023/A:1011234301664>.
- [10] N. Mohan, C.R. Mahesa, B.M. Rajaprakash, Erosive wear behaviour of WC filled glass epoxy composites, Procedia Eng. 68 (2013) 694–702, <https://doi.org/10.1016/j.proeng.2013.12.241>.
- [11] H.K. Dave, R.T. Karumuri, A.R. Prajapati, S.R. Rajpurohit, Specific energy absorption during compression testing of ABS and FPU parts fabricated using LCD-SLA based 3D printer, Rapid Prototyp. J. 28 (2022) 1530–1540, <https://doi.org/10.1108/RPJ-04-2021-0075>.
- [12] N. Dhakal, X. Wang, C. Espejo, A. Morina, N. Emami, Impact of processing defects on microstructure, surface quality, and tribological performance in 3D printed polymers, J. Mater. Res. Technol. 23 (2023) 1252–1272, <https://doi.org/10.1016/j.jmrt.2023.01.086>.
- [13] N. Vidakis, P. Mangelis, M. Petousis, N. Mountakis, V. Papadakis, A. Moutsopoulos, D. Tsikritzis, Mechanical reinforcement of ABS with optimized nano titanium nitride content for material extrusion 3D printing, Nanomaterials 13 (2023), <https://doi.org/10.3390/nano13040669>.
- [14] N. Vidakis, M. Petousis, A. Maniadi, E. Koudoumas, A. Vairis, J. Kechagias, Sustainable additive manufacturing: mechanical response of acrylonitrile-butadiene-styrene over multiple recycling processes, Sustainability 12 (2020), <https://doi.org/10.3390/su12093568>.
- [15] N.R. Madhu, H. Erfani, S. Jadoun, M. Amir, Y. Thiagarajan, N.P.S. Chauhan, Fused deposition modelling approach using 3D printing and recycled industrial materials for a sustainable environment: a review, Int. J. Adv. Des. Manuf. Technol. 122 (2022) 2125–2138, <https://doi.org/10.1007/s00170-022-10048-y>.
- [16] M.A.N. bin Mohd Khairul Nizam, K.I. bin Ismail, T.C. Yap, The effect of printing orientation on the mechanical properties of FDM 3D printed parts BT - enabling, in: A.S. Abdul Sani, M.N. Osman Zahid, M.R. Mohamad Yasin, S.Z. Ismail, M.Z. Mohd Zawawi, A.R. Abdul Manaf, S.N. Mohd Salleh, R. Abd Aziz, F. Mohd Turan (Eds.), Industry 4.0 through Advances in Manufacturing and Materials, Springer Nature Singapore, Singapore, 2022, pp. 75–85.
- [17] A. Vairis, M. Petousis, N. Vidakis, K. Savvakis, On the strain rate sensitivity of abs and abs plus fused deposition modeling parts, J. Mater. Eng. Perform. 25 (2016) 3558–3565, <https://doi.org/10.1007/s11665-016-2198-x>.
- [18] H. Zhang, L. Cai, M. Golub, Y. Zhang, X. Yang, K. Schlarman, J. Zhang, Tensile, creep, and fatigue behaviors of 3D-printed acrylonitrile butadiene styrene, J. Mater. Eng. Perform. 27 (2018) 57–62, <https://doi.org/10.1007/s11665-017-2961-7>.
- [19] D.G. Zisopoul, I. Nae, A.I. Portocarrero, I. Ramadan, A statistical approach of the flexural strength of PLA and ABS 3D printed parts, engineering, Technol. Appl. Sci. Res. 12 (2022) 8248–8252, <https://doi.org/10.48084/etas.4739>.
- [20] R. Vahed, H.R. Zarei Rajani, A.S. Milani, Can a black-box AI replace costly DMA testing?—a case study on prediction and optimization of dynamic mechanical properties of 3D printed acrylonitrile butadiene styrene, Materials 15 (2022), <https://doi.org/10.3390/ma15082855>.
- [21] N. Vidakis, M. Petousis, A. Vairis, K. Savvakis, A. Maniadi, A parametric determination of bending and Charpy's impact strength of ABS and ABS-plus fused deposition modeling specimens, Prog. Addit. Manuf. 4 (2019) 323–330, <https://doi.org/10.1007/s40964-019-00092-8>.
- [22] V.S. Vakharla, M. Singh, A. Salem, M.C. Halbig, J.A. Salem, Effect of reinforcements and 3-D printing parameters on the microstructure and mechanical properties of acrylonitrile butadiene styrene (ABS) polymer composites, Polymers 14 (2022), <https://doi.org/10.3390/polym14102105>.
- [23] N. V Blaž, L.D. Živanov, M.G. Kisić, A.B. Meničanin, Fully 3D printed rolled capacitor based on conductive ABS composite electrodes, Electrochim. Commun. 134 (2022), 107178, <https://doi.org/10.1016/j.elecom.2021.107178>.
- [24] M.K.H. R, M.G.M. Benal, G.S. P, V. Tambrallimath, H.R. G, T.M.Y. Khan, A. A. Rajhi, M.A. Baig, Influence of short glass fibre reinforcement on mechanical properties of 3D printed ABS-based polymer composites, Polymers 14 (2022), <https://doi.org/10.3390/polym14061182>.
- [25] H.R. M, M.G.M. Benal, G.S. P, V. Tambrallimath, K. Ramaiah, T.M.Y. Khan, J. K. Bhutto, M.A. Ali, Effect of short glass fiber addition on flexural and impact behavior of 3D printed polymer composites, ACS Omega 8 (2023) 9212–9220, <https://doi.org/10.1021/acsomega.2c07227>.
- [26] N. Vidakis, A. Maniadi, M. Petousis, M. Vamvakaki, G. Kenanakis, E. Koudoumas, Mechanical and electrical properties investigation of 3D-printed acrylonitrile-butadiene-styrene graphene and carbon nanocomposites, J. Mater. Eng. Perform. 29 (2020) 1909–1918, <https://doi.org/10.1007/s11665-020-04689-x>.

- [27] S. Dul, B.J.A. Gutierrez, A. Pegoretti, J. Alvarez-Quintana, L. Fambri, 3D printing of ABS Nanocomposites. Comparison of processing and effects of multi-wall and single-wall carbon nanotubes on thermal, mechanical and electrical properties, *J. Mater. Sci. Technol.* 121 (2022) 52–66, <https://doi.org/10.1016/j.jmst.2021.11.064>.
- [28] D.M. Bigg, Mechanical properties of particulate filled polymers, *Polym. Compos.* 8 (1987) 115–122, <https://doi.org/10.1002/pc.750080208>.
- [29] A.D. Valino, J.R.C. Dizon, A.H. Espera, Q. Chen, J. Messman, R.C. Advincula, Advances in 3D printing of thermoplastic polymer composites and nanocomposites, *Prog. Polym. Sci.* 98 (2019), 101162, <https://doi.org/10.1016/j.progpolymsci.2019.101162>.
- [30] N. Vidakis, A. Maniadi, M. Petousis, Maniadi, Mechanical Properties of 3D-Printed ABS with Combinations of Two Fillers: Graphene Nanoplatelets, TiO₂, ATO Nanocomposites and Zinc Oxide Micro, ZnOm, 2021.
- [31] A.B. Peters, C. Wang, D. Zhang, A. Hernandez, D.C. Nagle, T. Mueller, J.B. Spicer, Reactive laser synthesis of ultra-high-temperature ceramics HfC, ZrC, TiC, HfN, ZrN, and TiN for additive manufacturing, *Ceram. Int.* 49 (2023) 11204–11229, <https://doi.org/10.1016/j.ceramint.2022.11.319>.
- [32] İ. Aktifiz, K. Aydin, F. Darıcık, A. Topcu, Production of different metal oxide nanoparticle embedded polymer matrix composite structures by the additive manufacturing technology and investigation of their properties, *Polym. Compos.* 43 (2022) 7826–7835, <https://doi.org/10.1002/pc.26894>.
- [33] A. Maniadi, M. Vamvakaki, M. Petousis, N. Vidakis, M. Suchea, M. Sevastaki, Z. Viskadourakis, G. Kenanakis, E. Koudoumas, Effect of zinc oxide concentration on the dielectric properties of 3D printed acrylonitrile butadiene styrene nanocomposites, in: 2019 International Semiconductor Conference, CAS, 2019, pp. 221–224, <https://doi.org/10.1109/SMICND.2019.8923905>.
- [34] M. Petousis, N. Michailidis, V.M. Papadakis, A. Korlos, N. Mountakis, A. Argyros, E. Dimitriou, C. Charou, A. Moutsopoulos, N. Vidakis, Optimizing the rheological and thermomechanical response of acrylonitrile butadiene styrene/silicon nitride nanocomposites in material extrusion additive manufacturing, *Nanomaterials* 13 (2023) 1588, <https://doi.org/10.3390/nano13101588>.
- [35] M. Petousis, N. Vidakis, N. Mountakis, A. Moutsopoulos, V.M. Papadakis, E. Maravelakis, Emmanuel Maravelakis, On the substantial mechanical reinforcement of Polylactic Acid with Titanium Nitride ceramic nanofillers in material extrusion 3D printing, *Ceram. Int.* 49 (2023) 16397–16411, <https://doi.org/10.1016/j.ceramint.2023.02.001>.
- [36] X. Yang, S. Liang, X. Wang, P. Xiao, Z. Fan, Effect of WC and CeO₂ on microstructure and properties of W–Cu electrical contact material, *Int. J. Refract. Metals Hard Mater.* 28 (2010) 305–311, <https://doi.org/10.1016/j.ijrmhm.2009.11.009>.
- [37] H. Bai, L. Zhong, L. Kang, J. Liu, W. Zhuang, Z. Lv, Y. Xu, A review on wear-resistant coating with high hardness and high toughness on the surface of titanium alloy, *J. Alloys Compd.* 882 (2021), 160645, <https://doi.org/10.1016/j.jallcom.2021.160645>.
- [38] M.A. Moore, The relationship between the abrasive wear resistance, hardness and microstructure of ferritic materials, *Wear* 28 (1974) 59–68, [https://doi.org/10.1016/0043-1648\(74\)90101-X](https://doi.org/10.1016/0043-1648(74)90101-X).
- [39] A. Tidjani, O. Wald, M.-M. Pohl, M.P. Hentschel, B. Schartel, Polypropylene-graft-maleic anhydride-nanocomposites: I—characterization and thermal stability of nanocomposites produced under nitrogen and in air, *Polym. Degrad. Stabil.* 82 (2003) 133–140, [https://doi.org/10.1016/S0141-3910\(03\)00174-5](https://doi.org/10.1016/S0141-3910(03)00174-5).
- [40] Z. Movasaghi, S. Rehman, I.U. Rehman, Raman spectroscopy of biological tissues, *Appl. Spectrosc. Rev.* 42 (2007) 493–541, <https://doi.org/10.1080/05704920701551530>.
- [41] B.H. Stuart, Temperature studies of polycarbonate using Fourier transform Raman spectroscopy, *Polym. Bull.* 36 (1996) 341–346, <https://doi.org/10.1007/BF00319235>.
- [42] M. Makarem, C.M. Lee, K. Kafle, S. Huang, I. Chae, H. Yang, J.D. Kubicki, S.H. Kim, Probing cellulose structures with vibrational spectroscopy, *Cellulose* 26 (2019) 35–79, <https://doi.org/10.1007/s10570-018-2199-z>.
- [43] D. Giordano, J.K. Russell, D. González-García, D. Bersani, D.B. Dingwell, C. Del Negro, Raman spectroscopy from laboratory and proximal to remote sensing: a tool for the volcanological sciences, *Rem. Sens. (Basel)* 12 (2020), <https://doi.org/10.3390/rs12050805>.
- [44] V. Resta, G. Quarta, M. Lomascolo, L. Maruccio, L. Calcagnile, Raman and Photoluminescence spectroscopy of polycarbonate matrices irradiated with different energy 28Si⁺ ions, *Vacuum* 116 (2015) 82–89, <https://doi.org/10.1016/j.vacuum.2015.03.005>.
- [45] Z. Lin, X. Guo, Z. He, X. Liang, M. Wang, G. Jin, Thermal degradation kinetics study of molten polylactide based on Raman spectroscopy, *Polym. Eng. Sci.* 61 (2021) 201–210, <https://doi.org/10.1002/pen.25568>.
- [46] C. Zimmerer, I. Matulaitiene, G. Niaura, U. Reuter, A. Janke, R. Boldt, V. Sablinskas, G. Steiner, Nondestructive characterization of the polycarbonate - octadecylamine interface by surface enhanced Raman spectroscopy, *Polym. Test.* 73 (2019) 152–158, <https://doi.org/10.1016/j.polymertesting.2018.11.023>.
- [47] A.V. Spivak, Y.A. Litvin, A.V. Shushkanova, V.Y.u.S. Litvin, Diamond formation in carbonate-silicate-sulfide-carbon melts: Raman- and IR-microspectroscopy, *Eur. J. Mineral.* 20 (2008) 341–347, <https://doi.org/10.1127/0935-1221/2008/0020-1818>.
- [48] B.K.M. Luiz, R.D.M.C. Amboni, L.H.M. Prates, J. Roberto Bertolino, A.T.N. Pires, Influence of drinks on resin composite: evaluation of degree of cure and color change parameters, *Polym. Test.* 26 (2007) 438–444, <https://doi.org/10.1016/j.polymertesting.2006.12.005>.
- [49] E. Gatin, S.-M. Iordache, E. Matei, C.-R. Luculescu, A.-M. Iordache, C.E. A. Grigorescu, R.R. Ilici, Raman spectroscopy as spectral tool for assessing the degree of conversion after curing of two resin-based materials used in restorative dentistry, *Diagnostics* 12 (2022), <https://doi.org/10.3390/diagnostics12081993>.
- [50] J. Macedo, A. Samaro, V. Vanhoorne, C. Vervaet, J.F. Pinto, Processability of poly (vinyl alcohol) based filaments with paracetamol prepared by hot-melt extrusion for additive manufacturing, *J. Pharmaceut. Sci.* 109 (2020) 3636–3644, <https://doi.org/10.1016/j.xphs.2020.09.016>.
- [51] Y. Zare, Study of nanoparticle aggregation/agglomeration in polymer particulate nanocomposites by mechanical properties, *Compos Part A Appl Sci Manuf* 84 (2016) 158–164, <https://doi.org/10.1016/j.compositesa.2016.01.020>.
- [52] A. Tessema, D. Zhao, J. Moll, S. Xu, R. Yang, C. Li, S.K. Kumar, A. Kidane, Effect of filler loading, geometry, dispersion and temperature on thermal conductivity of polymer nanocomposites, *Polym. Test.* 57 (2017) 101–106, <https://doi.org/10.1016/j.polymertesting.2016.11.015>.
- [53] A. Kutvonen, G. Rossi, S.R. Puisto, N.K.J. Rostedt, T. Ala-Nissila, Influence of nanoparticle size, loading, and shape on the mechanical properties of polymer nanocomposites, *J. Chem. Phys.* 137 (2012), 214901, <https://doi.org/10.1063/1.4767517>.
- [54] M.M. Rueda, M.-C. Auscher, R. Fulchiron, T. Périé, G. Martin, P. Sonntag, P. Cassagnau, Rheology and applications of highly filled polymers: a review of current understanding, *Prog. Polym. Sci.* 66 (2017) 22–53, <https://doi.org/10.1016/j.progpolymsci.2016.12.007>.
- [55] L. Jiang, Y.C. Lam, K.C. Tam, T.H. Chua, G.W. Sim, L.S. Ang, Strengthening acrylonitrile-butadiene-styrene (ABS) with nano-sized and micron-sized calcium carbonate, *Polymer (Guildf)* 46 (2005) 243–252.
- [56] A. Saadat, H. Nazockdast, F. Sepehr, M. Mehranpour, Linear and nonlinear melt rheology and extrudate swell of acrylonitrile-butadiene-styrene and organoclay-filled acrylonitrile-butadiene-styrene nanocomposite, *Polym. Eng. Sci.* 50 (2010) 2340–2349, <https://doi.org/10.1002/pen.21769>.
- [57] H. Münschedt, Rheology of rubber-modified polymer melts, *Polym. Eng. Sci.* 21 (1981) 259–270, <https://doi.org/10.1002/pen.760210503>.
- [58] R. Arrigo, A. Frache, FDM printability of PLA based-materials: the key role of the rheological behavior, *Polymers* 14 (2022), <https://doi.org/10.3390/polym14091754>.
- [59] S. Tamayo-Vegas, A. Muhsan, C. Liu, M. Tarfaoui, K. Lafdi, The effect of agglomeration on the electrical and mechanical properties of polymer matrix nanocomposites reinforced with carbon nanotubes, *Polymers* 14 (2022), <https://doi.org/10.3390/polym14091842>.
- [60] S.A. Mostafa, A.S. Faried, A.A. Farighi, M.M. EL-Deeb, T.A. Tawfik, S. Majer, M. Abd Elrahman, Influence of nanoparticles from waste materials on mechanical properties, durability and microstructure of UHPC, *Materials* 13 (2020), <https://doi.org/10.3390/ma13204530>.
- [61] W. Ao, P. Liu, H. Liu, S. Wu, B. Tao, X. Huang, L.K.B. Li, Tuning the agglomeration and combustion characteristics of aluminized propellants via a new functionalized fluoropolymer, *Chem. Eng. J.* 382 (2020), 122987, <https://doi.org/10.1016/j.cej.2019.122987>.
- [62] M.K. Hassanzadeh-Aghdam, M.J. Mahmoodi, R. Ansari, Creep performance of CNT polymer nanocomposites -An emphasis on viscoelastic interphase and CNT agglomeration, *Compos. B Eng.* 168 (2019) 274–281, <https://doi.org/10.1016/j.compositesb.2018.12.093>.
- [63] N. Hamed, M.S. El-Feky, M. Kohail, E.-S.A.R. Nasr, Effect of nano-clay de-agglomeration on mechanical properties of concrete, *Construct. Build. Mater.* 205 (2019) 245–256, <https://doi.org/10.1016/j.conbuildmat.2019.02.018>.
- [64] I.-Y. Jeon, J.-B. Baek, Nanocomposites derived from polymers and inorganic nanoparticles, *Materials* 3 (2010) 3654–3674, <https://doi.org/10.3390/ma3063654>.
- [65] A. Tidjani, C.A. Wilkie, Photo-oxidation of polymeric-inorganic nanocomposites: chemical, thermal stability and fire retardancy investigations, *Polym. Degrad. Stabil.* 74 (2001) 33–37, [https://doi.org/10.1016/S0141-3910\(01\)00061-1](https://doi.org/10.1016/S0141-3910(01)00061-1).
- [66] K. Ullegaddi, Shivarudraiah, C.R. Mahesha, Significance of tungsten carbide filler reinforcement on ultimate tensile strength of basalt fiber epoxy composites, *Int. J. Recent Technol. Eng.* 8 (2019) 7913–7916, <https://doi.org/10.35940/ijrte.C6617.098319>.
- [67] F. Shahramforouz, S.M. Hejazi, A. Taherizadeh, Evaluating the tribological and mechanical properties of filament wound composite incorporated with PTFE fibers and tungsten carbide filler applicable for self-lubricating bearings, *Surf Topogr* 9 (2021), 35039, <https://doi.org/10.1088/2051-672X/ac22f2>.
- [68] M. Petousis, N. Michailidis, V.M. Papadakis, A. Korlos, N. Mountakis, A. Argyros, E. Dimitriou, C. Charou, A. Moutsopoulos, N. Vidakis, Optimizing the rheological and thermomechanical response of acrylonitrile butadiene styrene/silicon nitride nanocomposites in material extrusion additive manufacturing, *Nanomaterials* 13 (2023), <https://doi.org/10.3390/nano13101588>.
- [69] N. Gama, S. Magina, A. Ferreira, A. Barros-Timmons, Chemically modified bamboo fiber/ABS composites for high-quality additive manufacturing, *Polym. J.* 53 (2021) 1459–1467, <https://doi.org/10.1038/s41428-021-00540-9>.
- [70] B. Huang, H. He, S. Meng, Y. Jia, Optimizing 3D printing performance of acrylonitrile-butadiene-styrene composites with cellulose nanocrystals/silica nanohybrids, *Polym. Int.* 68 (2019) 1351–1360, <https://doi.org/10.1002/pi.5824>.
- [71] M.A. Osman, M.R.A. Atia, Investigation of ABS-rice straw composite feedstock filament for FDM, *Rapid Prototyp. J.* 24 (2018) 1067–1075, <https://doi.org/10.1108/RPJ-11-2017-0242>.